Spontaneous capillary propulsion of liquid droplets on substrates with nonuniform curvature

P. Galatola*
Université Paris Diderot, Sorbonne Paris Cité, Laboratoire Matière et Systèmes Complexes (MSC), UMR 7057 CNRS, F-75205 Paris, France

(Received 20 November 2017; published 5 October 2018)

A liquid droplet spread on a solid substrate with nonuniform curvature, in the absence of pinning, spontaneously moves. By means of a perturbative scheme, we determine analytically the speed of the droplet and the total capillary force acting on it, by assuming that the only relevant dissipation mechanism is the contact line viscosity. Our solution holds for droplets small with respect to the capillary length and in the limit where the curvature of the substrate is small with respect to the curvature of the droplet. By means of a numerical solution, we validate our perturbative calculation and determine its limit of validity. Our theoretical results are in agreement with recent experimental data on the movement of submillimeter-sized water droplets on conical glass pipettes [Lv *et al.*, Phys. Rev. Lett. **113**, 026101 (2014)].

DOI: 10.1103/PhysRevFluids.3.103601

I. INTRODUCTION

The surface tension γ between two substances is the energy cost per unit area for creating an interface between them [1]. Therefore, by dimensional analysis, the *capillary* force acting on a fluid droplet or volume is the product of γ and some characteristic length L. It is then expected that, whenever a gradient of γ or L is present, a net capillary force will arise and the fluid will be set in motion.

A classical example of fluid motion induced by a gradient of surface tension is the "tears of wine" phenomenon observed at the rim of a glass of strong wine or spirit [2]: since water has a much higher surface tension than alcohol, evaporation of the latter on the ridge of the meniscus leads to a surface tension gradient that raises, by the so-called Marangoni effect [3], a thin film along the glass sides. A similar transient movement occurs when a water droplet is deposited at the boundary between two substrates with different chemical treatments [4,5]. This movement can be made steady if the drop itself induces, by means of a chemical reaction, a gradient of surface tension with the substrate between the front and the rear of the drop [6,7]. A droplet can also be set in motion by means of a thermal gradient, due to the induced gradient of surface tension [8].

The situation in which the motion of a droplet is induced by a gradient of some characteristic length was studied, e.g., in Ref. [9], where it was shown that a drop, straddling around a conical fiber, spontaneously moves toward the region of lower curvature. A similar movement is found for a drop sitting on the *exterior* of a conical surface [10]. As already suggested by Bouasse a long time ago [11], a slug *inside* a conical capillary tube should instead move toward the region of higher curvature [10].

*paolo.galatola@univ-paris-diderot.fr

Apart from its fundamental interest, the spreading of liquid droplets on solid surfaces is important in many technological processes, ranging from inkjet printing to the passive positioning of liquids in the tanks of spacecrafts.

In this paper, by assuming that the only relevant dissipation mechanism is the contact line viscosity, we determine a general approximate analytical expression of the capillary force and speed for a liquid droplet spread on a non uniformly curved solid substrate. Our analytical results hold in the limit where the curvature of the substrate is small with respect to the curvature of the droplet, the latter being large with respect to the inverse capillary length. We validate our results by exact numerical computations and by comparisons with the experimental data of Lv *et al.* [10]. When the curvature gradient of the interface can be considered constant along the contact line with the droplet, our formula for the total capillary force coincides with the theoretical prediction of Lv *et al.* [10], that is based on energetic considerations for *equilibrium* droplets deposited on spherical substrates. However, as we shall show, the physical mechanism behind the movement of the droplet is the geometrical frustration induced by the constraint of constant mean curvature of the droplet surface. This constraint is imposed by the equilibrium between the liquid-vapor surface tension and the pressure jump across the surface of the droplet: It impedes the contact line from reaching a constant contact angle with the substrate, when the latter is nonuniformly curved, as it would be required for the droplet to be steady.

Our paper is organized as follows. To start with, we present our theoretical model in Sec. II. Then, for the sake of clarity, we directly skip in Sec. III to resuming our main perturbative results. In Sec. IV, we show that the experimental data of Lv *et al.* [10] are in agreement with our analytical solution. In Sec. V, we then compare the latter, for the case of a conical interface—as experimentally studied in Ref. [10]—with an exact numerical calculation, detailed in the Appendix. We consider the two situations in which the droplet sits either outside or inside the conical surface. For the latter case, the drop is found to move toward regions of larger curvature (i.e., the tip of the cone), in agreement with the early prediction of Bouasse [11]. In the following Sec. VI, we detail our perturbative scheme. Finally, in Sec. VII, we summarize our work and we conclude.

II. MODEL

To start with, let us introduce our model of the droplet dynamics. We consider a liquid droplet, of size small with respect to the capillary length [1], spread on a solid substrate. Moreover, let us suppose that the droplet, the substrate, and the ambient phase constitute a closed system that is in thermal and chemical equilibrium. Then, the free energy of the system $\mathcal{F}_\gamma$ contains only the surface tension contributions

$$\mathcal{F}_\gamma = \gamma \mathcal{A}_{\rm LV} + \gamma_{\rm LS}\mathcal{A}_{\rm LS} + \gamma_{\rm VS}\mathcal{A}_{\rm VS}, \tag{1}$$

where γ (respectively, $\gamma_{\rm LS}$ and $\gamma_{\rm VS}$) is the liquid-vapor (respectively, liquid-solid and vapor-solid) surface tension, and $\mathcal{A}_{\rm LV}$ (respectively, $\mathcal{A}_{\rm LS}$ and $\mathcal{A}_{\rm VS}$) is the area of the corresponding interface. At *equilibrium*, the contact angle Φ of the liquid-solid interface is equal to the Young angle Φ_Y, defined by the condition that the component parallel to the substrate of the resultant of the capillary forces acting on the liquid-solid-vapor triple line is zero [1]:

$$\gamma_{\rm VS} = \gamma_{\rm LS} + \gamma \cos \Phi_Y. \tag{2}$$

Note that when the contact angle Φ is larger (respectively, smaller) than Φ_Y, the triple contact line advances (respectively, recedes), i.e., the solid substrate is wetted (respectively, dewetted) by the liquid.

Since the total surface of the substrate $\mathcal{A}_{\rm LS} + \mathcal{A}_{\rm VS}$ is constant, using Eq. (2) we can rewrite the free energy (1), up to an irrelevant constant, as

$$\mathcal{F}_\gamma = \gamma \mathcal{A}_{\rm LV} - \gamma \cos \Phi_Y \mathcal{A}_{\rm LS}. \tag{3}$$

The constraint that the volume V of the droplet is equal to a constant value V_0 can be taken into account by defining the modified free energy

$$\mathcal{F} = \mathcal{F}_\gamma - P(V - V_0), \tag{4}$$

where the Lagrange multiplier P is equal to the pressure difference between the inside and the outside of the droplet.

As discussed by de Gennes [12], the spreading of a liquid on a solid substrate is accompanied by three types of dissipations: the viscous dissipation in the core of the liquid, the dissipation at the moving contact line, and the dissipation at the precursor film that is not a generic feature in the case of partial wetting [$|\cos\Phi_Y| \leqslant 1$ in Eq. (2)], in which we are interested. The dissipation at the contact line was first described by Cherry and Holmes [13] and Blake [14], in terms of the hopping motion of the fluid molecules at the edge of a droplet between adsorption sites distributed on the solid substrate.

In Ref. [15], de Ruijter *et al.* studied in detail the spreading dynamics of a droplet of di-n-butylphthalate on a polyethylene terephthalate (PET) substrate, in the regime of partial wetting. Except at very early times, they found that their experimental data are well fitted by taking into account only the dissipation of the contact line. For small velocities, this dissipation can be accounted for by means of a viscous force—per unit length of the contact line—that is proportional to the speed of the contact line. The coefficient of proportionality defines a line viscosity ζ [16] that has the same physical dimensions as a fluid dynamic viscosity, although its value generally differs from the latter. In the following, in agreement with these findings, we shall suppose that the only dissipation mechanism is the line viscosity.

The presence of defects on the substrate gives rise to a retentive force on the contact line that is the analogous for a liquid of the solid static friction [17]. Indeed, recent measurements by Nan Gao *et al.* [18] showed that, for different fluids and substrates, the initial dynamics of a sessile drop sitting on a solid substrate can be divided into a static and a kinetic regime, where the former is characterized by a threshold force needed to set the droplet in motion, and the latter can be described by a viscous friction. Since we are not interested in how the droplet is set into motion, in the following we shall suppose that the static retentive force can be neglected.

Our assumptions will be finally validated by comparison with experimental data [10]. However, we cannot exclude that, under different experimental conditions, the dissipation mechanisms that we neglected could be relevant. Even in the experimental situation of Ref. [10], it could be interesting to study in detail the effects of, e.g., the viscous dissipation mechanisms. However, developing such a complete hydrodynamical model is a formidable task that goes far beyond our goals.

Velocity-dependent dissipative forces that can be derived from a Rayleigh dissipation function $\mathcal{W}$ are easily incorporated in the Lagrangian formalism [19]. For a given Lagrangian coordinate q, the corresponding velocity-dependent generalized Lagrangian force F_q associated to $\mathcal{W}$ is $F_q = -\partial\mathcal{W}/\partial\dot{q}$, where $\dot{q} = \partial q/\partial t$ is the generalized speed (here and in the following we shall indicate by a dot the partial derivative with respect to time). The relationship between the velocity-dependent force F_q and the Rayleigh dissipation function $\mathcal{W}$ is thus analogous to the relationship between a conservative position-dependent force and its potential energy, with $\mathcal{W}$ replacing the potential energy and $\dot{q}$ replacing the coordinate q. In our case, to obtain a dissipative force that is linear in the speed of the contact line, we introduce the dissipation function quadratic in the speed of the contact line

$$\mathcal{W} = \frac{1}{2}\zeta \int (\boldsymbol{v} \cdot \hat{\boldsymbol{\nu}})^2 ds, \tag{5}$$

where ζ is the line viscosity, s is the arc length along the contact line, $\boldsymbol{v}$ is the speed of the contact line [i.e., $\boldsymbol{v}(s)$ is the speed of the point of the contact line at the arc length coordinate s], and $\hat{\boldsymbol{\nu}}$ is the normal to the contact line in the plane of the substrate. Note that the speed $\boldsymbol{v}$ depends on the way the contact line is parametrized: A component of $\boldsymbol{v}$ parallel to the contact line simply corresponds to a reparametrization of the curve, while its normal component $\boldsymbol{v} \cdot \hat{\boldsymbol{\nu}}$ is independent

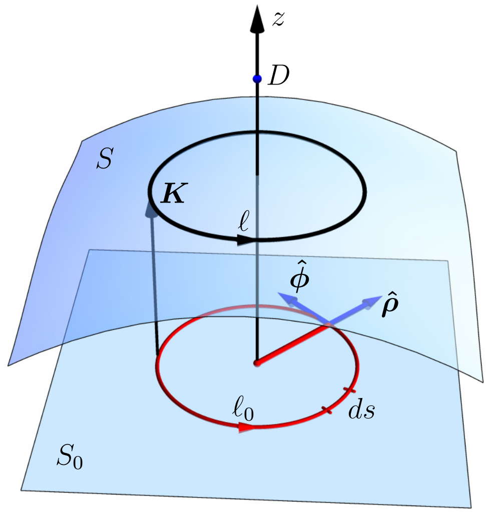

FIG. 1. Geometry for the calculation of the approximate speed and force when a droplet is spread on a curved substrate S. The reference plane S_0 is the tangent plane to S at the normal projection of the center of mass D of the droplet to the substrate S. For the sake of clarity, here S_0 has been shifted downward. The circle ℓ_0 is the equilibrium contact line when S coincides with S_0: It is centered with respect to the normal projection of D. The z axis is normal to S_0. The curvature tensor K of the substrate entering in the line integral in Eq. (7) is the curvature tensor of S on the curve ℓ, projection of ℓ_0 on S in the z direction.

of the parametrization and corresponds to a true displacement of the contact line. Equation (5) is the only functional quadratic in the speed of the contact line that is independent of the coordinate system and homogeneous with respect to all the points of the contact line. From a physical point of view, a dissipation function like (5), that depends quadratically on the speeds, is equal to half the dissipated power [19].

In the following, we shall further consider the viscous limit, in which the inertia of the droplet is negligible. Then, the dynamics of the system, described by the free energy $\mathcal{F}(\{q\})$ (4) (where $\{q\}$ is the set of all the Lagrangian coordinates) and the dissipation function $\mathcal{W}(\{q\}, \{\dot{q}\})$ (5), can be derived by extremizing the Rayleighian [19,20]

$$\mathcal{R} = \dot{\mathcal{F}} + \mathcal{W}, \tag{6}$$

with respect to the generalized speeds $\{\dot{q}\}$.

III. PERTURBATIVE RESULTS

By means of a first-order expansion in the small ratio between the curvature of the substrate and the curvature of the drop, in Sec. VI we shall show that, when the substrate S is nonuniformly curved, the drop, in general, moves. In this section, we anticipate our main theoretical findings.

Let us introduce a reference plane S_0 asymptotically close to S in the contact region between the drop and the substrate S. We shall take for S_0 the plane tangent to S at the normal projection of the center of mass D of the drop to the substrate S (see Fig. 1). If S is flat and thus coincides with S_0, at equilibrium the drop assumes a spherical cap shape with a polar aperture equal to the Young contact angle Φ_Y (2) and a radius a depending on its volume and on Φ_Y [see Eqs. (43) and (34)]. The corresponding contact line ℓ_0 is a circle of radius $a \sin \Phi_Y$. Indeed, for a flat substrate this geometry guarantees that the contact angle is everywhere equal to the equilibrium Young angle and that, according to Laplace law [1], the mean curvature of the surface of the drop is constant. As we shall show in Sec. VI, when the substrate S is curved, to first order in the ratio between the curvature of the substrate and the curvature of the droplet, the latter, under steady conditions, moves with the speed

$$\boldsymbol{v} = \frac{\gamma \sin \Phi_Y}{\pi \zeta} \oint_{\ell_0} (\boldsymbol{K} : \hat{\boldsymbol{\phi}} \otimes \hat{\boldsymbol{\phi}}) \hat{\boldsymbol{\rho}} \, ds. \tag{7}$$

Here $\boldsymbol{K}$ is the intrinsic curvature tensor of the substrate (47) at the points projection of ℓ_0 on S along the normal to S_0, ds is the line element of ℓ_0, and $\hat{\boldsymbol{\rho}}$ and $\hat{\boldsymbol{\phi}}$ are, respectively, the radial and tangent unit vectors to ℓ_0 (see Fig. 1). The product $\boldsymbol{K} : \hat{\boldsymbol{\phi}} \otimes \hat{\boldsymbol{\phi}}$ is the scalar curvature of the substrate in the direction of the unperturbed contact line ℓ_0. It is the tensor contraction on both indices of the symmetric tensors $\boldsymbol{K}$ and $\hat{\boldsymbol{\phi}} \otimes \hat{\boldsymbol{\phi}}$, where $\otimes$ is the tensorial product of two vectors. Therefore, indicating by K_{ij} and ϕ_i (with $i = 1, 2$) the Cartesian components of $\boldsymbol{K}$ and $\hat{\boldsymbol{\phi}}$, we have

$$\boldsymbol{K} : \hat{\boldsymbol{\phi}} \otimes \hat{\boldsymbol{\phi}} = \sum_{i,j=1}^{2} K_{ij} \phi_i \phi_j. \tag{8}$$

The total capillary force $\boldsymbol{F}$, parallel to the reference plane S_0, acting on the drop is proportional to its speed: $\boldsymbol{F} = \frac{1}{2} \zeta s_{\ell_0} \boldsymbol{v}$, where $s_{\ell_0} = 2\pi a \sin \Phi_Y$ is the length of the unperturbed contact line ℓ_0. The average force per unit length acting on the contact line is therefore equal to $\zeta \boldsymbol{v}/2$.

Equation (7) implies that a nonuniform curvature of the substrate generally gives rise to a propulsion of the droplet. This behavior can be explained by the fact that the equilibrium, at the surface of the droplet, of the liquid-vapor surface tension γ and of the pressure jump P across the droplet, forces, by Laplace law [1], the mean curvature H of the drop to be constant (32). Such a constant mean curvature is generally incompatible, for a nonuniformly curved substrate, with a constant contact angle—equal to the Young angle—that would be required in order that the contact line, in the absence of pinning, does not slide.

Note that the speed $\boldsymbol{v}$, as the force $\boldsymbol{F}$, linearly depends on the curvature tensor $\boldsymbol{K}$; therefore, reversing the curvature reverses the direction of motion. Moreover, the latter direction is independent of the Young angle Φ_Y.

If the curvature tensor $\boldsymbol{K}$ can be approximated, along the unperturbed contact line ℓ_0, by a linear development around the center $x = y = 0$ of ℓ_0, where x and y are Cartesian coordinates on the reference plane S_0,

$$\boldsymbol{K}(x, y) = \boldsymbol{K}_0 + \boldsymbol{K}_x x + \boldsymbol{K}_y y, \tag{9}$$

parametrizing the coordinates (x, y) of ℓ_0 in terms of the polar angle ϕ:

$$x = a \sin \Phi_Y \cos \phi, \tag{10}$$

$$y = a \sin \Phi_Y \sin \phi, \tag{11}$$

with

$$\hat{\boldsymbol{\phi}} = -\sin \phi \, \hat{\boldsymbol{x}} + \cos \phi \, \hat{\boldsymbol{y}}, \tag{12}$$

$$ds = a \sin \Phi_Y d\phi, \tag{13}$$

where $\hat{\boldsymbol{x}}$ and $\hat{\boldsymbol{y}}$ are the unit vectors in the x and y directions, respectively, and with $\hat{\boldsymbol{\rho}}$ given by Eq. (55), Eq. (7) can be approximated as

$$\boldsymbol{v} = \frac{\gamma a^2 \sin^3 \Phi_Y}{2\zeta} \nabla H|_{(x=0, y=0)}, \tag{14}$$

where $H = \frac{1}{2} \operatorname{Tr} \boldsymbol{K} = \frac{1}{2}(\kappa_1 + \kappa_2)$ is the mean curvature of the substrate, equal to the average between the two principal curvatures κ_1 and κ_2, and the gradient ∇H is computed at the center of

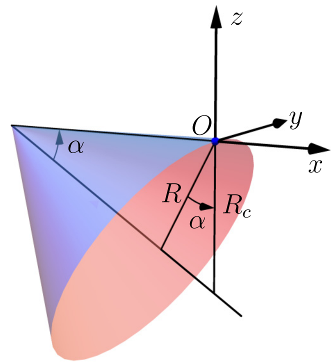

FIG. 2. Local coordinates for the calculation of the force and speed when a drop is spread on a conical surface of half aperture angle α. The origin of the coordinates O is the normal projection of the center of mass of the drop on the substrate. The x (respectively, y) axis is along the principal direction of zero (respectively, nonzero) curvature of the cone. The z axis is normal to the cone surface. R is the local radius of the circular section of the cone. R_c is the finite local radius of curvature of the cone.

the unperturbed contact line ℓ_0. Note that, to arrive at Eq. (14), we further used the approximation for the curvature tensor of a surface $z = z(x, y)$

$$\boldsymbol{K} = \begin{pmatrix} \frac{\partial^2 z}{\partial x^2} & \frac{\partial^2 z}{\partial x \partial y} \\ \frac{\partial^2 z}{\partial x \partial y} & \frac{\partial^2 z}{\partial y^2} \end{pmatrix}, \tag{15}$$

valid to first order in z, coherently with the approximation, that we used to arrive at Eq. (7), of a substrate the curvature of which is small with respect to the curvature of the droplet, such that the droplet shape is close to a spherical cap [see Eq. (35)]. The corresponding force coincides with the result of Lv *et al.* [10] that was obtained by energetic considerations for *equilibrium* droplets spread on spherical substrates.

IV. COMPARISON WITH THE EXPERIMENTAL DATA

To test our analytical model, we fit the experimental data of Lv *et al.* [10] on the speed of micrometer-sized droplets deposited on conical surface-treated glass pipettes.

We call α the half aperture angle of the right circular conical substrate. For a given point O on the surface of the cone, we introduce a local Cartesian coordinate system with origin in O, x axis parallel to the generatrix passing through O and directed away from the vertex, y axis tangent to the cone, and z axis in the direction of the outward normal to the cone (see Fig. 2). The x and y axes are then parallel, respectively, to the zero and nonzero principal curvature directions of the cone. The local finite radius of curvature R_c of the substrate is linked to the local radius R of the circular section of the cone by the relation (see Fig. 2)

$$R = R_c \cos\alpha. \tag{16}$$

In this local frame, to lowest order in x and y for $x, y \ll R_c$, the equation of the cone is

$$z = \frac{y^2}{2R_c}\left(\frac{x\tan\alpha}{R_c} - 1\right) + \mathcal{O}(y^4) + \mathcal{O}(x^2y^2). \tag{17}$$

In particular, from this expression it is easily verified that in O ($x = y = 0$), the principal curvatures of the surface, that correspond to the eigenvalues of the $\boldsymbol{K}$ matrix (15), are 0 and $-1/R_c$, in the x and y directions, respectively.

By symmetry, a droplet deposited on this conical surface, with normal projection of its center of mass on the surface in O, under steady conditions will move along the x direction. According to Eqs. (14)–(17) and using Eqs. (43) and (34) to express the unperturbed radius a of the droplet in terms of its volume V_0 and of the Young angle Φ_Y, the x components of the force and of the speed are given by

$$F_x = \frac{3\gamma V_0 \sin(2\alpha)\cos^4\left(\frac{\Phi_Y}{2}\right)}{2R^2(2+\cos\Phi_Y)}, \tag{18}$$

$$v_x = \frac{\gamma \sin(2\alpha)\sin^3\Phi_Y}{8\zeta R^2}\left[\frac{3V_0}{4\pi(2+\cos\Phi_Y)\sin^4\left(\frac{\Phi_Y}{2}\right)}\right]^{2/3}. \tag{19}$$

In the experimental data of Lv *et al.* [10], the inertia of the droplets is not negligible. We then suppose that the acceleration of the drop is driven by the capillary force (18) and by a viscous reaction force proportional to its speed, such that the stationary speed coincides with (19). Using the relationship $dR/dt = \sin\alpha\, dx/dt$ (see Fig. 2), the equation of motion of the droplet can then be cast in the form

$$\frac{dv}{dR} = \frac{3\gamma\cos\alpha\cos^4(\Phi_Y/2)}{\rho(2+\cos\Phi_Y)vR^2} - \frac{\zeta\sin\Phi_Y}{\rho\sin\alpha}\left[\frac{3\pi^2}{4V_0^2(2+\cos\Phi_Y)\sin^4(\Phi_Y/2)}\right]^{1/3}, \tag{20}$$

where $v = dx/dt$ is the x component of the speed of the droplet and ρ is its mass per unit volume. Note that this equation of motion differs from the analysis of Lv *et al.* [10] only by the dissipation mechanism, that in Ref. [10] is taken into account by means of a contact angle hysteresis model. We fit the experimental points of Fig. 1(b) of Ref. [10] by numerically solving the differential equation (20). We fix $\rho = 1 \times 10^3\,\mathrm{kg\,m^3}$ and $\gamma = 80\,\mathrm{mN\,m^{-1}}$ for the water droplets and we use for α and V_0 the values given in Ref. [10] for each one of the four set of experimental data. Then, the theoretical speed $v^{\mathrm{th}}(R)$ at the cone radius R, obtained by integrating Eq. (20), depends on the initial speed v_0 corresponding to the smallest measured $R = R_{\min}$ value, on the unknown line viscosity ζ and on the Young angle Φ_Y. We introduce the total χ^2 error

$$\chi^2 = \sum_{i=1}^{m}\left[\left(\frac{v^{\mathrm{th}}(R_i+\delta_i) - v_i^{\exp}}{\sigma_i}\right)^2 + \left(\frac{\delta_i}{\sigma_i'}\right)^2\right], \tag{21}$$

where m is the number of experimental points and σ_i (respectively, σ_i') is the experimental error on the measured speed $v_i^{\exp}$ (respectively, measured radius R_i) of the ith point. We then minimize numerically, by means of a simplex algorithm [21], χ^2 with respect to δ_i (with $i = 1,\ldots,m$), v_0, ζ, and Φ_Y to yield the sought best fit. As shown in Fig. 3, a quite good agreement between the experimental data and our theoretical prediction is found, particularly for the first two curves starting from the top. The fixed and minimization parameters and the χ^2 per point of the fits are indicated in the caption of the figure. In particular, the inferred values for the line viscosity ζ vary between 9.85×10^{-3} Pa s and 2.26×10^{-2} Pa s and are compatible with the typical values obtained by applying a molecular-kinetic theory to experimental data for various systems [22,23].

However, as already found in Ref. [10], the values of the Young angles given by the fits significantly differ from the statically measured ones (from top to bottom of Fig. 3, $\Phi_Y = 10^\circ$, 10°, 15°, and 40°, respectively) and seem rather to correspond to the typical initial contact angles of the droplets, just after deposition (see Fig. 1(a) of Ref. [10]). This discrepancy can be explained by the spreading dynamics of the droplets. Indeed, as it will be shown in Sec. VI D, before reaching the stationary speed (7), the droplets have to relax to a quasistationary shape, independent of the initial conditions. Now, as will be shown in Sec. V (see Fig. 5), at least for slightly (at the droplet scale) curved substrates, when the droplets have not yet relaxed to their quasistationary shape—so that the average contact angle significantly differ from the Young angle—the actual speed and

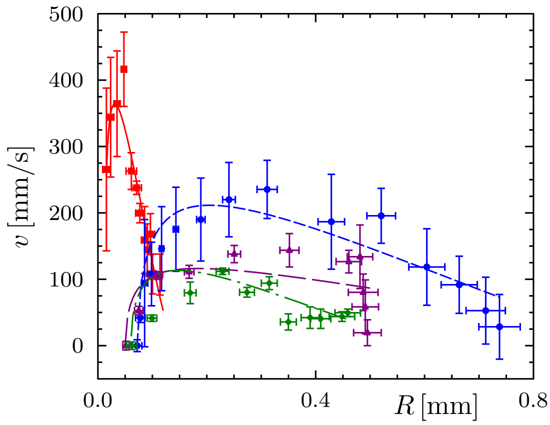

FIG. 3. Comparison between the experimental speeds of the droplets (points with error bars deduced from Fig. 1(b) of Ref. [10]) and the analytical model of Eq. (20) (lines), as a function of the local radius R of the circular section of the conical substrate. From top to bottom, squares and red full line: $V_0 = 1.15 \times 10^{-2}\,\text{mm}^3$, $\alpha = 5.1^\circ$, $\Phi_Y = 143.3^\circ$, $\zeta = 2.17 \times 10^{-2}\,\text{Pa s}$, $v_0 = 256.8\,\text{mm/s}$, $R_{\text{min}} = 1.56 \times 10^{-2}\,\text{mm}$, $\chi^2 = 0.55$ per point; circles and blue short-dashed line: $V_0 = 1\,\text{mm}^3$, $\alpha = 3.2^\circ$, $\Phi_Y = 136.5^\circ$, $\zeta = 1.63 \times 10^{-2}\,\text{Pa s}$, $v_0 = 3.5 \times 10^{-3}\,\text{mm/s}$, $R_{\text{min}} = 7.21 \times 10^{-2}\,\text{mm}$, $\chi^2 = 0.46$ per point; triangles and purple long-dashed line: $V_0 = 1\,\text{mm}^3$, $\alpha = 3.2^\circ$, $\Phi_Y = 153.4^\circ$, $\zeta = 9.85 \times 10^{-3}\,\text{Pa s}$, $v_0 = 6.7 \times 10^{-3}\,\text{mm/s}$, $R_{\text{min}} = 5 \times 10^{-2}\,\text{mm}$, $\chi^2 = 3.64$ per point; and diamonds and green dot-dashed line: $V_0 = 1\,\text{mm}^3$, $\alpha = 3.2^\circ$, $\Phi_Y = 149.7^\circ$, $\zeta = 2.26 \times 10^{-2}\,\text{Pa s}$, $v_0 = 2.5 \times 10^{-3}\,\text{mm/s}$, $R_{\text{min}} = 6 \times 10^{-2}\,\text{mm}$, $\chi^2 = 4.97$ per point.

force are indeed close to our analytical formula, but with the Young angle replaced by the average instantaneous contact angle, which depends on the initial conditions.

In the linear regime, for curvatures of the substrate small with respect to those of the droplet, and for shapes close to the spherical cap equilibrium shape for a flat substrate, the typical relaxation time τ for spreading is given by Eq. (72). With the ζ values obtained by the fits, the volumes V_0 of the drops, and the above cited experimental values of the equilibrium Young angles, we then obtain the relaxation times, for the situations corresponding to the curves in Fig. 3, $\tau = 3.93$, 13.1, 3.10, and 0.812 ms, respectively, from top to bottom. On the other hand, the corresponding time lapses from the first point in Fig. 3 to the point of maximum speed, computed on the fitted solutions, are 0.516, 15.1, 26.8, and 18.9 ms, respectively. We then see that, at least for the first two curves, the linear relaxation time is large or comparable to the time it takes to accelerate the drop to its maximum speed. For the last two curves, instead, the linear relaxation time is small with respect to the time to the maximum speed, although not completely negligible. This intermediate situation, plus the fact that nonlinear corrections, both in the spreading and in the drifting dynamics, are expected to be not negligible for such droplets—that are rather big with respect to the typical radii of the conical substrate—is the likely reason for the relatively poor fit. Taking into account other possible dissipation mechanisms, such as hydrodynamic dissipation, could improve the fit with the experimental data. However, given the error bars of the experimental data, such an analysis seems rather delicate and is out of the scopes of the present work.

Finally, note that we tried to add to the right-hand side of the equation of motion (20) a term proportional to $-1/v$ that represents the effect of a static pinning force on the contact line. However, within the accuracy of the fit, the pinning force turns out to be zero.

V. COMPARISON BETWEEN THE ANALYTICAL AND THE NUMERICAL SOLUTIONS

The analytical results (7) and (14) hold in the limit in which the curvature of the substrate is negligible with respect to the curvature of the droplet. Moreover, in this limit, as discussed in

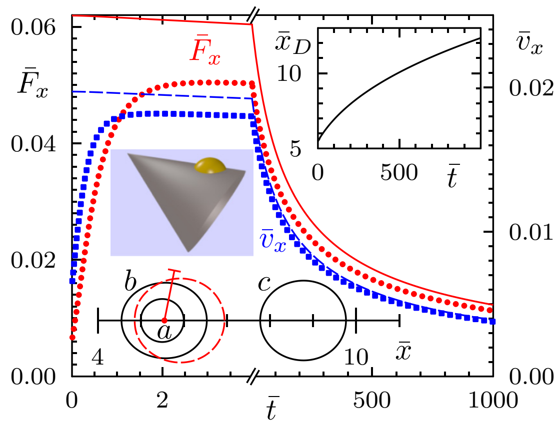

FIG. 4. Normalized force $\bar{F}_x$ and speed of the contact line $\bar{v}_x$ as a function of the normalized time $\bar{t}$, for droplets with Young angle $\Phi_Y = 60^\circ$ spread on the outer surface of a cone of half aperture angle $\alpha = 20^\circ$. Note the two different scales of the broken $\bar{t}$ axis. Red circles, numerically computed normalized force acting on the drop (left vertical scale); and blue squares, numerically computed normalized speed of the contact line (right vertical scale). The red continuous (respectively, blue dashed) line is the analytical approximation (18) [respectively, (19)] at the numerically computed center of mass $\bar{x}_D(t)$ of the droplet. The evolution of the latter as a function of the normalized time $\bar{t}$ is shown in the upper right inset. The origin of the $\bar{x}$ axis is at the vertex of the cone. Lower inset: projection of the contact line on the tangent plane $(\bar{x}, \bar{y})$. Curve a, $\bar{t} = 0$ (initial condition, circle of radius 0.5); curve b, $\bar{t} = 3$; and curve c, $\bar{t} = 300$. The dashed red line shows a polar plot of the contact angle for the b contact line at $\bar{t} = 3$: The center of the plot is the center of the contact line (red dot). The contact line corresponds to a contact angle equal to the Young angle $\Phi_Y = 60^\circ$; a 1-deg variation corresponds to the shown radial distance between the contact line and the red tick on the radial line [thus, e.g., on the front (respectively, back) of the drop, the contact angle is $\simeq 61.4^\circ$ (respectively, $\simeq 59.0^\circ$)]. Middle left inset: three-dimensional view of the droplet for $\bar{t} = 200$.

Sec. VI D, the dynamics of a droplet consists of two distinct phases: a rapid transient during which the drop spreads to reach a quasistationary shape independent of the initial conditions, followed by a slow drift. In order to verify these predictions, we determine numerically—as detailed in the Appendix—the exact dynamics, according to our model (see Sec. II), of a droplet spread on an arbitrarily curved substrate.

Throughout all this section, lengths are normalized with respect to the radius r_0 of the equilibrium circular contact line when the droplet is spread on a flat interface, time is normalized with respect to the characteristic time $\zeta r_0/\gamma$, and forces with respect to γr_0. All the normalized quantities are denoted by a bar.

For the sake of definiteness, we consider, as in the experiment of Lv *et al.* [10], a right circular conical substrate. In Fig. 4, we show the dynamical evolution of a droplet with Young angle $\Phi_Y = 60^\circ$ spread on the external surface of a cone of half aperture angle $\alpha = 20^\circ$. The $\bar{x}$, $\bar{y}$, and $\bar{z}$ axes are oriented as in Fig. 2, with origin of the axes on the vertex of the cone. The initial condition at $\bar{t} = 0$ corresponds to a contact line, the projection of which on the tangent plane $(\bar{x}, \bar{y})$ to the substrate is a circle of normalized radius 0.5, centered on the point $(\bar{x} = \bar{R}_c/\tan\alpha, \bar{y} = 0)$ of the conical surface with normalized radius of curvature $\bar{R}_c = 2$.

The points in the main panel of Fig. 4 show the numerically determined time evolution of the $\bar{x}$ axis components of the normalized force $\bar{F}_x$ (red dots, vertical left scale) and speed $\bar{v}_x$ (blue squares, vertical right scale), the $\bar{y}$ components being zero because of the symmetry of the substrate and of the initial condition. The lines show the corresponding analytical approximations [red continuous line for the force (18), blue dashed line for the speed (19)]. The latter are computed, at each time $\bar{t}$, in correspondence to the numerically determined normal projection of the center of mass of the droplet on the substrate ($\bar{x} = \bar{x}_D(\bar{t})$, $\bar{y} = 0$). The evolution of $\bar{x}_D$ as a function of the reduced time $\bar{t}$ is shown in the upper right inset of Fig. 4. Note that the speed $\bar{v}_x$, both in the numerical and in the analytical solution, is computed as the speed of the frame moving with the drop in such a way that the $n = 1$ Fourier harmonics of the radial shape of the contact line remain constant (zero in the present case). Indeed, adding small $n = 1$ Fourier harmonics to the radial shape of an almost circular contact line amounts to a rigid translation. The so-computed speed of the contact line practically coincides, when the curvature of the substrate is small with respect to the curvature of the droplet, with the speed of the center of mass of the latter.

At short times (note the two different timescales of the broken $\bar{t}$ axis of the main panel), as the droplet spreads, the force and speed rapidly increase to reach quasistationary values independent of the initial conditions. At $\bar{t} = 4$, the analytical approximation for the force is some 20% higher than the exact numerical solution, while the analytical approximation for the speed is only about 7% higher than the exact one. This error is due to the fact that here the nonzero normalized principal curvature of the substrate on the contact area with the droplet is of the order of 0.5, only less than a factor of two smaller than the characteristic curvature of the droplet. This actually shows that our approximate solution holds even when the curvature of the substrate becomes comparable to the curvature of the droplet.

At larger times, the force and the speed decrease, since the droplet drifts away from the vertex of the cone (see the upper right inset), where the curvatures and their gradients are smaller. At the same time, the analytical approximations improve. Note that although in the approximate perturbative solution the speed of the drop and the force acting on it are proportional, this is not true for the exact numerical solution. Indeed, even if there is a local proportionality between the viscous force on the contact line and its local speed, the shape of the droplet and of its contact line varies when the speed changes, thus introducing a nonlinearity of geometrical origin between the speed of the droplet and the force acting on it.

The lower inset of Fig. 4 shows the shape of the contact line, projected onto the ($\bar{x}$, $\bar{y}$) plane, tangent to the conical surface, at three different times: $\bar{t} = 0$ (curve a), $\bar{t} = 3$ (curve b), and $\bar{t} = 300$ (curve c). The evolution of these shapes illustrates the initial rapid spread of the drop to a quasistationary shape, independent of the initial conditions, followed by the slow drift. The dashed red line centered on the b contact line is a polar plot of the corresponding contact angle. More precisely, the contact angle at a given position of the black contact line b can be read by measuring the difference in radial coordinate, with respect to the center of the contact line (red dot), between the dashed red curve and the contact line b. When the dashed curve coincides with the contact line, the contact angle is equal to the equilibrium Young angle $\Phi_Y = 60^\circ$. The red tick drawn on the shown radial direction indicates a +1-deg variation for the corresponding point on the contact line. So, e.g., the contact angle at the front of the drop (i.e., on the right intersection with the $\bar{x}$ axis) is $\simeq 61.4^\circ$, while at the rear (on the left intersection) it is $\simeq 59.0^\circ$. This asymmetry in contact angles between the front and the rear of the drop explains why the droplet moves: Indeed (see Sec. II), when the contact angle is larger (respectively, smaller) than the Young angle, the contact line advances (respectively, recedes). In turn, as we said, the contact angle asymmetry arises from the constraint of constant mean curvature of the droplet surface, because of Laplace law [1]. This constraint is incompatible, for a general surface geometry, with a constant contact angle.

We illustrate the dynamics of spreading and drifting of the droplet in the videos in the Supplemental Material [24]. In particular, Movie 1 [24] shows the dynamics corresponding to Fig. 4 from $\bar{t} = 0$ to $\bar{t} = 2$. On the video, 1 s corresponds to a normalized time lapse $\Delta\bar{t} = 0.1$. To highlight the drifting, Movie 2 [24] shows the full evolution displayed in Fig. 4, from $\bar{t} = 0$ to $\bar{t} = 1000$, accelerated by a factor of 1000 with respect to Movie 1 (1 s of video corresponding now to $\Delta\bar{t} = 100$).

Since the force and the speed linearly depend on the curvature tensor of the substrate, a droplet deposited *inside* the conical surface drifts toward the tip of the cone, as illustrated in Movie 3 and Movie 4 [24]. In particular, Movie 3 shows the time evolution from $\bar{t} = 0$ to $\bar{t} = 2$ for a droplet

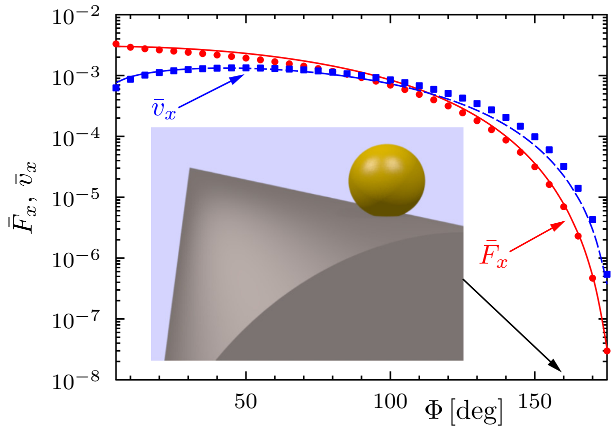

FIG. 5. Numerically determined normalized force $\bar{F}_x$ (red circles) and speed of the contact line $\bar{v}_x$ (blue squares) as a function of the angle Φ defining the radius of the circular projection of the contact line on the $(\bar{x}, \bar{y})$ plane, tangent to the conical substrate. The latter projection coincides with the contact line of the droplet on a flat interface when the Young angle is equal to Φ. The inset shows the equilibrium shape of the droplet for the value $\Phi = 160^\circ$, indicated by the arrow. The Young angle is $\Phi_Y = 10^\circ$, the half-aperture angle of the cone is $\alpha = 5^\circ$, and the nonzero normalized radius of the circular section of the cone at the center of the contact line is $\bar{R} = 2$. The red continuous (respectively, blue dashed) line is the analytical approximation (18) [respectively, (19)] computed for $\Phi_Y = \Phi$.

with the same Young angle $\Phi_Y = 60^\circ$ and the same initial projection of the contact line on the $(\bar{x}, \bar{y})$ plane as in Fig. 4, but deposited *inside* a cone with the same half-aperture $\alpha = 20^\circ$. The radius of curvature at the center of the contact line at $\bar{t} = 0$ is equal to $\bar{R}_c = 5$. The timescale of the movie is the same as in Movie 1 (1 s corresponds to a normalized time lapse $\Delta\bar{t} = 0.1$). The corresponding drifting of the droplet, from $\bar{t} = 0$ to $\bar{t} = 1000$, is shown in Movie 4 (as in Movie 2, here 1 s corresponds to a normalized time lapse $\Delta\bar{t} = 100$).

To test the force and the speed under unsteady conditions, we consider a drop spread on the outer side of our conical surface with a given instantaneous contact line. We choose the latter such that its projection on the tangent plane $(\bar{x}, \bar{y})$ coincides with the equilibrium contact line of the droplet on a flat interface with Young angle equal to Φ. This is a circle, that we take centered at $\bar{x} = \bar{R}/\sin\alpha$, $\bar{y} = 0$. With this choice, the contact angle of the equilibrium shape of the droplet on the cone oscillates around Φ. The points in Fig. 5 show the numerically computed capillary force $\bar{F}_x$ (red dots) and instantaneous speed $\bar{v}_x$ of the contact line (blue squares) as a function of Φ. The Young angle is $\Phi_Y = 10^\circ$, the half-aperture angle of the cone is $\alpha = 5^\circ$, and the normalized radius of the circular section of the cone at the center of the contact line is $\bar{R} = 2$. As is shown in Fig. 5, the exact numerical force and speed are very close to the approximations (18) and (19) with the Young angle Φ_Y replaced by the angle Φ. This shows that, by replacing the Young angle with the average dynamic contact angle, our approximate solution gives, for not too curved interfaces and for drop shapes not too far from a spherical cap, a good estimate of the force and the speed also for unsteady situations, thus justifying the fits of Fig. 3.

Finally, to quantify the accuracy of the analytical approximation, we have numerically computed the relative error ΔF_x in the force and Δv_x in the speed, once the transient spreading has elapsed, for droplets spread outside or inside a conical surface. The relative error is here defined as the difference between the analytical approximation and the numerical solution divided by the absolute value of the latter. In Fig. 6 we show ΔF_x (upper panel *a*) and Δv_x (lower panel *b*) as a function of the normalized nonzero principal curvature $\bar{\kappa}$ of the conical surface. Negative (respectively, positive) values of $\bar{\kappa}$ correspond to the droplet being spread outside (respectively, inside) the conical surface. As in Fig. 4, the analytical force and speed are computed at the normal projection of the center of

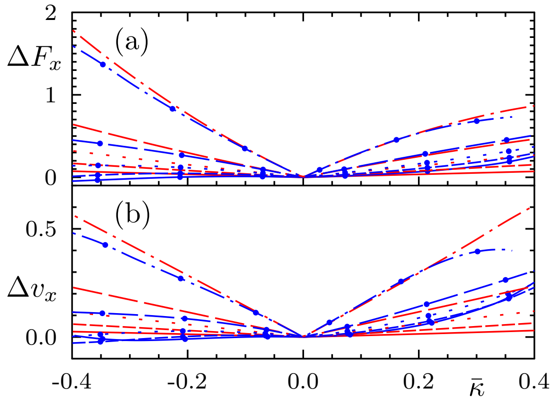

FIG. 6. Relative error in the force ΔF_x (a) and in the speed Δv_x (b) as a function of the normalized nonzero principal curvature $\bar{\kappa}$ of the cone. Negative (respectively, positive) values of $\bar{\kappa}$ correspond to the drop being outside (respectively, inside) the cone. Red lines, $\alpha = 5^\circ$; blue lines with dots, $\alpha = 60^\circ$; continuous lines, $\Phi_Y = 30^\circ$; short-dashed lines, $\Phi_Y = 60^\circ$; dotted lines, $\Phi_Y = 90^\circ$; long-dashed lines, $\Phi_Y = 120^\circ$; and dash-dotted lines: $\Phi_Y = 150^\circ$. Note that the blue curves with dots ($\alpha = 60^\circ$) for $\Phi_Y = 150^\circ$ stop slightly before $\bar{\kappa} = 0.4$ because the drop begins to touch the tip of the cone.

mass of the droplet on the substrate. The red lines (respectively, blue lines with dots) correspond to a cone of half aperture angle $\alpha = 5^\circ$ (respectively, $\alpha = 60^\circ$). For each value of α, five values of the Young angle are shown: $\Phi_Y = 30^\circ$, 60°, 90°, 120°, and 150° (from bottom to top close to $\bar{\kappa} = 0$). As is apparent, the error in the speed is always smaller (by a factor of about 3) than the error in the total force. These errors globally increase with the absolute value of the substrate curvature and with increasing Young angles but do not depend much on the aperture angle of the cone. Note that for small values of the Young angle $\Phi_Y \simeq 30^\circ$, the error in our approximation remains smaller than 10% even for curvatures of the order of one half of the typical curvatures of the droplet.

Again, note that Figs. 6(a) and 6(b) illustrate the fact that although the dissipation mechanism is linear, the total exact dissipation force *is not* linearly proportional to the speed of the drop. This is only true in the approximate perturbative calculation: Therefore, the relative errors in the force and in the speed generally differ.

VI. ANALYTICAL APPROXIMATION IN THE QUASIPLANAR CASE

In this section, we finally detail our perturbative analysis of the dynamics of a droplet spread on a quasiplanar substrate. To start with, we introduce a spherical coordinate system (r, θ, ϕ), where, with respect to a right-handed (x, y, z) Cartesian coordinate system, r is the radial distance from the origin $x = y = z = 0$, θ is the polar angle with respect to the z axis, and ϕ is the azimuthal angle with respect to the x axis in the (x, y) plane (see Fig. 7). Note that this system of coordinates—and, in particular, the choice of its origin with respect to the droplet (see Sec. VI A)—differ from those used in Sec. III to summarize the theoretical results and explicitly compute the speed and force for a droplet sliding on a conical surface. At a given time t, we parametrize the surface of the liquid droplet according to

$$r = r(\theta, \phi, t). \tag{22}$$

Similarly, we parametrize the fixed solid substrate on which the droplet lies as

$$r = h(\theta, \phi). \tag{23}$$

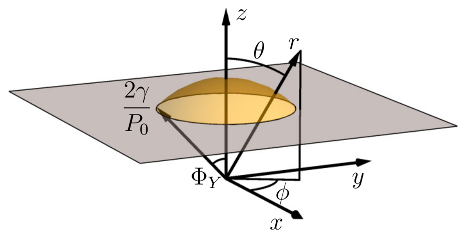

FIG. 7. System of coordinates used for the calculation of the analytical approximate solution around the shown unperturbed droplet of spherical cap shape lying on an unperturbed planar substrate.

The free energy (4) can then be written as

$$\mathcal{F} = \int_0^{2\pi} d\phi \int_0^{\theta(\phi,t)} d\theta \bigg[\gamma r \sqrt{\left(r^2 + r_\theta^2\right)\sin^2\theta + r_\phi^2} - \gamma \cos\Phi_Y h \sqrt{\left(h^2 + h_\theta^2\right)\sin^2\theta + h_\phi^2} + \frac{1}{3} P (h^3 - r^3) \sin\theta \bigg] + P V_0, \tag{24}$$

where subscripts indicate partial derivatives (i.e., $r_\theta = \partial r/\partial\theta$, etc.), $\theta = \theta(\phi, t)$ is the shape of the contact line, and we suppose that $\theta(\phi, t) < \pi/2$ [25]. Note that the pressure is a function of time: $P = P(t)$. Similarly, the dissipation function (5) becomes

$$\mathcal{W} = \frac{1}{2}\zeta \int_0^{2\pi} d\phi \, \frac{h^2 \dot\theta^2 \left[\left(h^2 + h_\theta^2\right)\sin^2\theta + h_\phi^2\right]}{\sqrt{h^2\left(\sin^2\theta + \theta_\phi^2\right) + (h_\theta \theta_\phi + h_\phi)^2}}, \tag{25}$$

where $\dot\theta = \partial\theta/\partial t$ is the time derivative of the contact line $\theta = \theta(\phi, t)$, $\theta_\phi = \partial\theta/\partial\phi$ is its derivative with respect to the azimuthal angle ϕ, and h and its derivatives are evaluated on the contact line $\theta = \theta(\phi, t)$.

The dynamical equations of the droplet are obtained by setting to zero the variation $\delta(\dot{\mathcal{F}} + \mathcal{W})$ of the Rayleighian (6) with respect to the generalized speeds $\dot r = \partial r(\theta, \phi, t)/\partial t$, $\dot\theta = \partial\theta(\phi, t)/\partial t$, and $\dot P = dP(t)/dt$. Taking into account the contact condition between the droplet and the substrate

$$r(\theta(\phi, t), \phi, t) = h(\theta(\phi, t), \phi) \tag{26}$$

on the contact line $\theta(\phi, t)$, we then easily obtain, by integrating by parts, the bulk equation

$$\frac{\partial}{\partial\theta}\left(\frac{\gamma r r_\theta \sin^2\theta}{S}\right) + \frac{\partial}{\partial\phi}\left(\frac{\gamma r r_\phi}{S}\right) - \gamma S - \frac{\gamma r^2 \sin^2\theta}{S} + P r^2 \sin\theta = 0, \tag{27}$$

with

$$S = \sqrt{\left(r^2 + r_\theta^2\right)\sin^2\theta + r_\phi^2}, \tag{28}$$

the boundary condition on the contact line $\theta = \theta(\phi, t)$

$$\frac{\zeta h^2 T^2 \dot\theta}{\sqrt{h^2\left(\sin^2\theta + \theta_\phi^2\right) + (h_\theta\theta_\phi + h_\phi)^2}} + \frac{\gamma r r_\theta (h_\theta - r_\theta)\sin^2\theta}{S} + \gamma r S - \gamma\cos\Phi_Y h\, T = 0, \tag{29}$$

with

$$T = \sqrt{\left(h^2 + h_\theta^2\right)\sin^2\theta + h_\phi^2}, \tag{30}$$

and the constraint that the volume of the droplet is equal to the constant value V_0

$$V_0 = \int_0^{2\pi} d\phi \int_0^{\theta(\phi,t)} d\theta \left[\frac{1}{3}(r^3 - h^3)\sin\theta\right]. \tag{31}$$

It can be checked that the bulk equation (27) expresses the Laplace equation [1], according to which the pressure difference P between the inside and the outside of the drop is proportional to the mean curvature H of the drop:

$$P = 2\gamma H. \tag{32}$$

Similarly, the dynamical equation (29) states that the normal speed of the contact line times the line viscosity ζ is equal to the unbalanced capillary force per unit length parallel to the substrate $\gamma_{\mathrm{LS}} + \gamma\cos\Phi - \gamma_{\mathrm{VS}} = \gamma(\cos\Phi - \cos\Phi_Y)$, where Φ is the contact angle.

A. Perturbative solution

When the substrate is plane, the equilibrium shape of the droplet is a spherical cap, with a contact angle equal to the Young angle Φ_Y (see Fig. 7). To obtain a perturbative solution for a substrate close to a plane, we introduce a fictitious small parameter $\epsilon \ll 1$ and we develop the shape of the droplet to first order in ϵ as

$$r(\theta,\phi,t) = \frac{2\gamma}{P_0}[1 + \epsilon\rho(\theta,\phi,t)], \tag{33}$$

where P_0 is the pressure difference between the inside of the unperturbed spherical cap and the outside and

$$a = \frac{2\gamma}{P_0} \tag{34}$$

is, by Laplace law, the radius of the unperturbed equilibrium spherical shape. Similarly, to first order in ϵ, we describe the shape of the solid substrate as

$$h(\theta,\phi) = \frac{2\gamma}{P_0\cos\theta}\cos\Phi_Y[1 + \epsilon\eta(\theta,\phi)], \tag{35}$$

where the function $\eta(\theta,\phi)$ describes the variation of the substrate from the plane $z = 2\gamma\cos\Phi_Y/P_0$ intersecting the spherical drop at the Young angle Φ_Y (see Fig. 7). We also develop the contact line around the circle of polar angle Φ_Y, corresponding to the unperturbed equilibrium situation, as

$$\theta(\phi,t) = \Phi_Y + \epsilon f(\phi,t). \tag{36}$$

Finally, we develop the pressure difference P between the inside and the outside of the drop as

$$P = P_0[1 + \epsilon p(t)]. \tag{37}$$

To first order in ϵ, the bulk equation (27) gives the linear partial differential equation that the drop perturbation $\rho(\theta,\phi,t)$ must obey:

$$\frac{\partial^2\rho}{\partial\theta^2} + \frac{1}{\tan\theta}\frac{\partial\rho}{\partial\theta} + \frac{1}{\sin^2\theta}\frac{\partial^2\rho}{\partial\phi^2} + 2(\rho + p) = 0. \tag{38}$$

Developing the contact condition (26) at first order in ϵ, we can express the perturbation of the contact line $f(\phi,t)$ as a function of the perturbations $\rho(\theta,\phi,t)$ and $h(\theta,\phi)$ as

$$f(\phi,t) = \frac{\rho(\theta = \Phi_Y,\phi,t) - \eta(\theta = \Phi_Y,\phi)}{\tan\Phi_Y}. \tag{39}$$

Finally, using this relationship, the boundary condition (29) gives, at first order in ϵ, the dynamical equation of the contact line

$$\left.\frac{\partial \rho}{\partial t}\right|_{\theta=\Phi_Y} = \frac{P_0}{2\zeta} \sin \Phi_Y [\cos \Phi_Y(\rho - \eta) + \sin \Phi_Y(\cos^2 \Phi_Y \eta_\theta - \rho_\theta)]_{\theta=\Phi_Y}. \tag{40}$$

To solve Eq. (38), we develop the drop perturbation $\rho(\theta, \phi, t)$ in the Fourier series in the azimuthal angle ϕ as

$$\rho(\theta, \phi, t) = -p(t) + \alpha_0(t) R_0(\theta) + \sum_{m=1}^{\infty} [\alpha_m(t)\cos(m\phi) + \beta_m(t)\sin(m\phi)] R_m(\theta). \tag{41}$$

Substituting this expression in Eq. (38) and setting $\xi = \cos\theta$, it is easily found that the solutions $R_m(\xi)$ that are regular at $\theta = 0$ for $m = 0$ and $m = 1$ are the associated Legendre functions of the first kind $P_1^m(\xi)$ [26], while for $m \geqslant 2$ they are linear combinations of the associated Legendre functions of the second kind $Q_1^m(\xi)$ and $Q_{-2}^m(\xi)$ [26] (with a singularity at the point $\theta = \pi$ outside the domain of the droplet). For any value of $m \geqslant 0$, these solutions, apart from an arbitrary multiplicative factor, can be expressed as

$$R_m(\theta) = (m + \cos\theta) \tan^m\left(\frac{\theta}{2}\right). \tag{42}$$

Note that $R_0 = \cos\theta$ and $R_1 = \sin\theta$. The value of $p(t)$, that determines the pressure difference (37), is fixed by the constant volume condition (31). Indeed, the latter, to zero order in ϵ, gives the volume V_0 of the droplet as a function of the Young angle Φ_Y and of the pressure difference P_0 [i.e., the unperturbed radius of the drop (34)]

$$V_0 = \frac{4\pi}{3}\left(\frac{2\gamma}{P_0}\right)^3 (2 + \cos\Phi_Y) \sin^4\left(\frac{\Phi_Y}{2}\right). \tag{43}$$

Imposing that the first-order correction in ϵ to the right-hand side of Eq. (31) is zero, gives then, with the development (41),

$$p(t) = \cos^2\left(\frac{\Phi_Y}{2}\right)\alpha_0(t) - \frac{\cos^3\Phi_Y}{4\pi \sin^2\left(\frac{\Phi_Y}{2}\right)} \int_0^{2\pi} d\phi \int_0^{\Phi_Y} \frac{\sin\theta\, \eta(\theta, \phi)}{\cos^3\theta} d\theta. \tag{44}$$

B. Speed of the drop

Substituting the general equilibrium solution for the shape of the droplet (41), (42), and the correction to the pressure jump (44) in the dynamical equation of the contact line (40), we obtain the time evolution equations for the coefficients $\alpha_m(t)$ and $\beta_m(t)$ defining the shape of the droplet. Note that, for $\epsilon \ll 1$, the coefficient $\alpha_1(t)$ [respectively, $\beta_1(t)$] describes a *rigid* translation of the droplet of a quantity $x_0 = 2\gamma\epsilon\alpha_1/P_0$ (respectively, $y_0 = 2\gamma\epsilon\beta_1/P_0$) along the x (respectively, y) direction. It then turns out that the horizontal speed $v_x = \dot{x}_0$, $v_y = \dot{y}_0$ of the droplet *only depends on the shape of the substrate* according to

$$v_x = \frac{\epsilon\gamma \cos\Phi_Y}{\pi\zeta} \int_0^{2\pi} d\phi \cos\phi \left[\frac{1}{2}\sin(2\Phi_Y)\eta_\theta - \eta\right]_{\theta=\Phi_Y}, \tag{45}$$

$$v_y = \frac{\epsilon\gamma \cos\Phi_Y}{\pi\zeta} \int_0^{2\pi} d\phi \sin\phi \left[\frac{1}{2}\sin(2\Phi_Y)\eta_\theta - \eta\right]_{\theta=\Phi_Y}. \tag{46}$$

To express the horizontal speed in a covariant form, let us introduce the intrinsic curvature tensor $\boldsymbol{K}$ of the substrate [27]

$$\boldsymbol{K} = \begin{pmatrix} \hat{\boldsymbol{n}} \cdot \frac{\partial^2 \boldsymbol{r}}{\partial u^2} & \hat{\boldsymbol{n}} \cdot \frac{\partial^2 \boldsymbol{r}}{\partial u \partial v} \\ \hat{\boldsymbol{n}} \cdot \frac{\partial^2 \boldsymbol{r}}{\partial u \partial v} & \hat{\boldsymbol{n}} \cdot \frac{\partial^2 \boldsymbol{r}}{\partial v^2} \end{pmatrix}, \tag{47}$$

where $\boldsymbol{r}(u, v)$ is the three-dimensional vector that specifies the points of the surface in terms of the arbitrary parameters u and v and

$$\hat{\boldsymbol{n}} = \frac{\frac{\partial \boldsymbol{r}}{\partial u} \times \frac{\partial \boldsymbol{r}}{\partial v}}{\left| \frac{\partial \boldsymbol{r}}{\partial u} \times \frac{\partial \boldsymbol{r}}{\partial v} \right|} \tag{48}$$

is the unit normal to the interface. The symmetric tensor $\boldsymbol{K}$ allows us to express the normal curvature $\kappa_n = \hat{\boldsymbol{n}} \cdot d\hat{\boldsymbol{s}}/ds$ of a curve lying on a surface in terms of the matrix product $\boldsymbol{t}^T \boldsymbol{K} \boldsymbol{t}$ [27]. Here s is the curvilinear coordinate of a curve $u = u(s)$, $v = v(s)$ lying on the surface and $\hat{\boldsymbol{s}}$ is the unit vector tangent to the curve. It can be expressed as

$$\hat{\boldsymbol{s}} = \boldsymbol{e}^T \boldsymbol{t}, \tag{49}$$

where

$$\boldsymbol{e} = \begin{pmatrix} \frac{\partial \boldsymbol{r}}{\partial u} \\ \frac{\partial \boldsymbol{r}}{\partial v} \end{pmatrix} \tag{50}$$

is the column vector containing the tangent vectors to the surface, T indicates transposition, and the column vector $\boldsymbol{t}$ contains the components of $\hat{\boldsymbol{s}}$ in the (u, v) basis

$$\boldsymbol{t} = \begin{pmatrix} \frac{du}{ds} \\ \frac{dv}{ds} \end{pmatrix}. \tag{51}$$

Note that the normal curvature κ_n depends only on the geometry of the surface and the direction of the curve. In tensorial notation $\kappa_n = \boldsymbol{K} : \boldsymbol{t} \otimes \boldsymbol{t}$, where : indicates tensor contraction over all the indices and $\otimes$ is the tensorial product. Note finally that the eigenvalues of $\boldsymbol{K}$ are the principal curvatures of the interface and the corresponding eigenvectors give the components of their directions along $\boldsymbol{e}$ [27].

Using the parametrization (35), to first order in ϵ, with $u = \theta$ and $v = \phi$, the curvature tensor (47) of the substrate is

$$\boldsymbol{K} = \frac{2\epsilon\gamma \cos \Phi_Y}{P_0} \begin{pmatrix} \eta_{\theta\theta} - 2\eta_\theta \tan\theta & \eta_{\theta\phi} - \frac{2\eta_\phi}{\sin(2\theta)} \\ \eta_{\theta\phi} - \frac{2\eta_\phi}{\sin(2\theta)} & \eta_{\phi\phi} + \frac{\eta_\theta}{2}\sin(2\theta) \end{pmatrix}, \tag{52}$$

where $\eta_{\theta\theta} = \partial^2\eta/\partial\theta^2$, etc. The unperturbed circular contact line has elementary length element (see Fig. 7)

$$ds = \frac{2\gamma}{P_0} \sin \Phi_Y d\phi. \tag{53}$$

Then, the orthoradial unit vector $\hat{\boldsymbol{\phi}}$, tangent to the unperturbed circular contact line $(\theta = \Phi_Y, \phi)$, according to Eq. (51) has components in the (θ, ϕ) basis

$$\hat{\boldsymbol{\phi}} = \begin{pmatrix} 0 \\ \frac{P_0}{2\gamma \sin \Phi_Y} \end{pmatrix}. \tag{54}$$

Finally, introducing the radial unit vector, orthogonal to the unperturbed circular contact line,

$$\hat{\boldsymbol{\rho}} = \cos\phi\, \hat{\boldsymbol{x}} + \sin\phi\, \hat{\boldsymbol{y}}, \tag{55}$$

where $\hat{\boldsymbol{x}}$ and $\hat{\boldsymbol{y}}$ are the unit vectors in the x and y directions, respectively, it is easily seen, by means of two integrations by parts in the periodic coordinate ϕ, that the speed of the droplet [(45) and (46)], to first order in ϵ, can be expressed according to Eq. (7).

C. Horizontal force on the drop

The horizontal force acting on the drop is the sum of the components tangent to the substrate of the capillary forces acting on the contact line. It can be computed in terms of a stress tensor. To this aim, let us suppose that the drop and the substrate can be described, in Cartesian coordinates, by their heights $z(x, y)$ and $\bar{z}(x, y)$, respectively, with respect to a reference plane (x, y). Then, the free energy (4) becomes

$$\mathcal{F} = \int_{\Omega} [\gamma\sqrt{1 + (\nabla z)^2} - \gamma \cos\Phi_Y \sqrt{1 + (\nabla\bar{z})^2} + P(\bar{z} - z)] d^2r + PV_0, \tag{56}$$

where Ω is the projection of the drop on the reference plane (x, y), $d^2r = dx\,dy$ is the area element of the latter, and ∇ is the two-dimensional gradient operator. We now compute the variation of (56) with respect to an arbitrary variation δz of z and a displacement $\delta\boldsymbol{a}$ of the projection $\partial\Omega$ of the contact line on the reference plane. By means of an integration by parts, we obtain

$$\begin{aligned}\delta\mathcal{F} = &-\int_{\Omega} \left\{\nabla \cdot \left[\frac{\gamma\nabla z}{\sqrt{1 + (\nabla z)^2}}\right] + P\right\}\delta z\, d^2r \\ &+ \gamma \oint_{\partial\Omega} \left\{\frac{\nabla z \cdot \boldsymbol{\nu}\, \delta z}{\sqrt{1 + (\nabla z)^2}} + [\sqrt{1 + (\nabla z)^2} - \cos\Phi_Y\sqrt{1 + (\nabla\bar{z})^2}]\delta\boldsymbol{a} \cdot \boldsymbol{\nu}\right\} ds,\end{aligned} \tag{57}$$

where $\boldsymbol{\nu}$ is the unit normal to $\partial\Omega$ pointing outward with respect to Ω and ds is the elementary length of $\partial\Omega$. If $\boldsymbol{r}_{\partial\Omega}$ is a point of $\partial\Omega$, the contact condition between the drop and the substrate implies that $z(\boldsymbol{r}_{\partial\Omega}) = \bar{z}(\boldsymbol{r}_{\partial\Omega})$. Then, if $z'(x, y) = z(x, y) + \delta z(x, y)$ is the varied shape of the drop, we must also have $z'(\boldsymbol{r}_{\partial\Omega} + \delta\boldsymbol{a}) = \bar{z}(\boldsymbol{r}_{\partial\Omega} + \delta\boldsymbol{a})$. Developing this last condition to first order in δz and $\delta\boldsymbol{a}$ and using the former then gives the relationship

$$\delta z(\boldsymbol{r}_{\partial\Omega}) = (\nabla\bar{z} - \nabla z) \cdot \delta\boldsymbol{a}. \tag{58}$$

Substituting Eq. (58) in the contour integral in the right-hand side of Eq. (57), we finally obtain

$$\delta\mathcal{F} = -\int_{\Omega} \left\{\nabla \cdot \left[\frac{\gamma\nabla z}{\sqrt{1 + (\nabla z)^2}}\right] + P\right\}\delta z\, d^2r - \oint_{\partial\Omega} \delta\boldsymbol{a} \cdot \boldsymbol{\Sigma} \cdot \boldsymbol{\nu}\, ds, \tag{59}$$

where

$$\boldsymbol{\Sigma} = \gamma\frac{(\nabla z - \nabla\bar{z}) \otimes \nabla z}{\sqrt{1 + (\nabla z)^2}} - \gamma\sqrt{1 + (\nabla z)^2}\,\mathbf{1} + \gamma\cos\Phi_Y\sqrt{1 + (\nabla\bar{z})^2}\,\mathbf{1} \tag{60}$$

is the stress tensor, being $\mathbf{1}$ the identity tensor. Indeed, for an equilibrium drop shape, $\delta\mathcal{F}$ must vanish for a fixed contact line ($\delta\boldsymbol{a} = \mathbf{0}$) and an arbitrary variation δz of the drop shape. Then, the term in square brackets in Eq. (59) must vanish, which gives the equilibrium equation defining the shape of the drop for a fixed contact line. The variation of the free energy for an equilibrium drop due to a displacement of the contact line is then given by the contour line integral in Eq. (59). This variation is equal to the total *external* work that must be done on the system to displace the drop. Writing this work as

$$\delta F = -\oint_{\partial\Omega} \boldsymbol{f} \cdot \boldsymbol{\delta a}\, ds, \tag{61}$$

where $\boldsymbol{f}\, ds$ is the component of the *internal* elementary force parallel to the reference plane (x, y) acting on the contact line, since $\delta\boldsymbol{a}$ is arbitrary, we see that $\boldsymbol{f} = \boldsymbol{\Sigma} \cdot \boldsymbol{\nu}$. The total internal force acting on the drop parallel to the reference plane (x, y) is then

$$\boldsymbol{F} = \oint_{\partial\Omega} \boldsymbol{\Sigma} \cdot \boldsymbol{\nu}\, ds. \tag{62}$$

With $x = r \sin\theta \cos\phi$, $y = r \sin\theta \sin\phi$, $z = r \cos\theta$ and the radial distances (33) and (35) for the drop and the substrate, respectively, at first order in ϵ we get

$$\begin{aligned}\boldsymbol{F} &= \frac{\epsilon\gamma^2 \sin(2\Phi_Y)}{P_0} \int_0^{2\pi} \left[\frac{\sin(2\Phi_Y)}{2}\eta_\theta - \eta\right]_{\theta=\Phi_Y} \hat{\boldsymbol{\rho}}\, d\phi \\ &\quad + \frac{2\epsilon\gamma^2 \sin\Phi_Y}{P_0} \int_0^{2\pi} (\cos\Phi_Y \rho - \sin\Phi_Y \rho_\theta)_{\theta=\Phi_Y} \hat{\boldsymbol{\rho}}\, d\phi. \end{aligned} \tag{63}$$

According to the development in Eqs. (41) and (42), the second integral in the right-hand side of Eq. (63) vanishes. Thus, the total force $\boldsymbol{F}$ is proportional to the drop speed $\boldsymbol{v}$: $\boldsymbol{F} = \pi\zeta a \sin\Phi_Y \boldsymbol{v}$, where a is the radius (34) of the drop on the unperturbed flat substrate.

D. Spreading of the drop

The Fourier harmonics $m \neq 0$ in the azimuthal angle ϕ of the dynamical equation (40) of the contact line describe the transient spreading of the drop to a stationary shape that only depends on the shape of the substrate.

Explicitly, the zero harmonic gives the evolution equation for the coefficient α_0, that, for $\epsilon \ll 1$, corresponds to a rigid translation of the drop of the quantity $2\gamma\epsilon\alpha_0/P_0$ along z,

$$\begin{aligned}\dot{\alpha}_0(t) &= \frac{P_0}{2\zeta}\Bigg(-\sin\Phi_Y(2+\cos\Phi_Y)\alpha_0(t) + \frac{\sin(2\Phi_Y)}{8\pi\sin^2\left(\frac{\Phi_Y}{2}\right)}\Bigg\{\int_0^{2\pi} d\phi[2\eta - \sin(2\Phi_Y)\eta_\theta]_{\theta=\Phi_Y} \\ &\quad - \frac{\cos^3\Phi_Y}{\sin^2\left(\frac{\Phi_Y}{2}\right)} \int_0^{2\pi} d\phi \int_0^{\Phi_Y} \frac{\sin\theta\, \eta(\theta,\phi)}{\cos^3\theta} d\theta\Bigg\}\Bigg). \end{aligned} \tag{64}$$

This equation describes the exponential relaxation of $\alpha_0(t)$ to the stationary value

$$\begin{aligned}\alpha_{0\infty} &= \frac{\cos\Phi_Y}{4\pi(2+\cos\Phi_Y)\sin^2\left(\frac{\Phi_Y}{2}\right)}\Bigg\{\int_0^{2\pi} d\phi[2\eta - \sin(2\Phi_Y)\eta_\theta]_{\theta=\Phi_Y} \\ &\quad - \frac{\cos^3\Phi_Y}{\sin^2\left(\frac{\Phi_Y}{2}\right)} \int_0^{2\pi} d\phi \int_0^{\Phi_Y} \frac{\sin\theta\, \eta(\theta,\phi)}{\cos^3\theta} d\theta\Bigg\} \end{aligned} \tag{65}$$

with the characteristic time constant

$$\tau_0 = \frac{\zeta a}{\gamma \sin\Phi_Y(2+\cos\Phi_Y)}, \tag{66}$$

where a is the radius (34) of the unperturbed drop. Similarly, the higher order harmonics $m \geqslant 2$ satisfy the evolution equations

$$\begin{aligned}\dot{\alpha}_m(t) &= \frac{P_0 \sin\Phi_Y}{2\zeta(m+\cos\Phi_Y)}\Bigg\{-(m^2-1)\alpha_m(t) \\ &\quad + \frac{\cos\Phi_Y}{\pi\tan^m\left(\frac{\Phi_Y}{2}\right)} \int_0^{2\pi} \left[\frac{1}{2}\sin(2\Phi_Y)\eta_\theta - \eta\right]_{\theta=\Phi_Y} \cos(m\phi) d\phi\Bigg\}, \end{aligned} \tag{67}$$

$$\dot{\beta}_m(t) = \frac{P_0 \sin \Phi_Y}{2\zeta(m + \cos \Phi_Y)} \Bigg\{ -(m^2 - 1)\beta_m(t) + \frac{\cos \Phi_Y}{\pi \tan^m \left(\frac{\Phi_Y}{2}\right)} \int_0^{2\pi} \left[\frac{1}{2} \sin(2\Phi_Y)\eta_\theta - \eta \right]_{\theta=\Phi_Y} \sin(m\phi) d\phi \Bigg\}. \quad (68)$$

Again, these equations describe the exponential relaxation of $\alpha_m(t)$ and $\beta_m(t)$ to the stationary values, respectively,

$$\alpha_{m\infty} = \frac{\cos \Phi_Y}{\pi(m^2 - 1)\tan^m \left(\frac{\Phi_Y}{2}\right)} \int_0^{2\pi} \left[\frac{1}{2} \sin(2\Phi_Y)\eta_\theta - \eta \right]_{\theta=\Phi_Y} \cos(m\phi) d\phi, \quad (69)$$

$$\beta_{m\infty} = \frac{\cos \Phi_Y}{\pi(m^2 - 1)\tan^m \left(\frac{\Phi_Y}{2}\right)} \int_0^{2\pi} \left[\frac{1}{2} \sin(2\Phi_Y)\eta_\theta - \eta \right]_{\theta=\Phi_Y} \sin(m\phi) d\phi, \quad (70)$$

with the characteristic time constants

$$\tau_m = \frac{\zeta a(m + \cos \Phi_Y)}{\gamma \sin \Phi_Y (m^2 - 1)}. \quad (71)$$

The largest value between (66) and (71), of the order of

$$\tau = \frac{\zeta a}{\gamma \sin \Phi_Y}, \quad (72)$$

determines the equilibration time for the local shape of the droplet.

Taking into account that our approximation is valid for a mean curvature $H \ll 1/a$ that varies slowly on a size $a \sin \Phi_Y$ of the order of the contact line radius, such that $|\nabla H| \ll 1/(a^2 \sin \Phi_Y)$ in the approximation (14), according to Eq. (14) the time that it takes for the droplet to move of a quantity of the order of the contact line radius is much larger than (72). Then, when our approximation holds, the droplet rapidly spreads on the timescale (72), reaching a local stationary state, and then slowly drifts with the speed (7), keeping a shape that depends on the local geometry of the substrate, according to Eqs. (33), (41), (42), (44), (65), (69), and (70).

VII. CONCLUSIONS

To conclude, by means of a perturbative approach, we have determined a general analytical approximation for the force and speed of a liquid droplet spread on an arbitrarily curved interface. We have assumed that the only dissipation mechanism that plays a relevant role is the contact line viscosity. Our approximation holds, under steady conditions, for droplets small with respect to the capillary length, such that gravity can be neglected, and when the typical radii of curvature of the substrate are large with respect to the size of the droplet. When the curvature gradient of the interface is almost constant along the contact line with the droplet, we recover for the total capillary force the result of Lv *et al.* [10], that was obtained by means of energetic considerations for *equilibrium* droplets spread on spherical surfaces.

We have shown that the physical mechanism behind the movement of the droplet is the constraint of constant mean curvature of the surface of the droplet, imposed by the Laplace law. This constraint frustrates, on an arbitrarily curved substrate, the contact angle from reaching a constant value equal to the equilibrium Young angle, as would be required for the droplet to remain still.

Our model fits the experimental data of Lv *et al.* [10]. However, under different experimental situations, other dissipation mechanisms that we neglected could be relevant. Even in the experimental situation of Ref. [10], it could be interesting to study in detail the effects of, e.g., the viscous dissipation mechanisms, by performing precise measurements under more controlled conditions.

We have checked our results and their limits of validity by means of extensive exact numerical calculations. Finally, we have shown that our analytical model can explain also the force and speed observed under nonsteady conditions, provided that the shape of the droplet remains close to a spherical cap.

ACKNOWLEDGMENT

I wish to thank Cunjing Lv for having suggested the problem and for fruitful discussions.

APPENDIX: EXACT NUMERICAL SOLUTION

In this Appendix, we present the approach that we used to numerically solve the model, introduced in Sec. II, of the time evolution of a droplet on a curved substrate. To start with, we introduce a set of cylindrical coordinates (r, z, ϕ) [28] and we describe the shape of the droplet at time t by means of the parametric equations [29]

$$r = r(u, \phi, t), \tag{A1}$$

$$z = z(u, \phi, t), \tag{A2}$$

where the parameter $u \in [0, 1]$ measures the curvilinear abscissa s of the curve obtained by intersecting the surface of the drop with the half-plane $\phi = \text{const}$ in units of its total length $s_0(\phi, t)$

$$u = \frac{s}{s_0(\phi, t)} \tag{A3}$$

(see Fig. 8). We take $u = 0$ on the contact line and $u = 1$ on the top of the droplet, at the intersection with the z axis. We further introduce the angle ψ that the tangent to the line obtained by intersecting the surface of the drop with the half-plane $\phi = \text{const}$ forms with respect to the radial direction r and the angle χ that the outward unit normal $\hat{\boldsymbol{n}}$ to the surface of the drop forms with the half-plane $\phi = \text{const}$. Explicitly, the angles ψ and χ are related to the shape of the drop in Eqs. (A1) and (A2) by the relationships

$$\frac{\partial r}{\partial u} = s_0 \cos\psi, \tag{A4}$$

$$\frac{\partial z}{\partial u} = s_0 \sin\psi, \tag{A5}$$

$$\tan\chi = \frac{1}{r}\left(\cos\psi \frac{\partial z}{\partial \phi} - \sin\psi \frac{\partial r}{\partial \phi}\right), \tag{A6}$$

while the Cartesian coordinates of $\hat{\boldsymbol{n}}$ are

$$\hat{\boldsymbol{n}} = \begin{pmatrix} \cos\chi \sin\psi \cos\phi - \sin\chi \sin\phi \\ \cos\chi \sin\psi \sin\phi + \sin\chi \cos\phi \\ -\cos\chi \cos\psi \end{pmatrix}. \tag{A7}$$

With these definitions, the free energy of the drop (4) becomes

$$\begin{aligned} \mathcal{F} = & \int_0^{2\pi} d\phi \int_0^1 du \left(\frac{\gamma s_0 r}{\cos\chi} - \frac{1}{2} P r^2 s_0 \sin\psi \right) - \gamma \cos\Phi_Y \int_0^{2\pi} d\phi \int_0^{r(u=0,\phi,t)} dr\, r \sqrt{1 + g_r^2 + \frac{1}{r^2} g_\phi^2} \\ & + P \int_0^{2\pi} d\phi \left[\int_0^{r(u=0,\phi,t)} dr\, r g(r,\phi) - \frac{1}{2} r^2(u=0,\phi,t) g(r(u=0,\phi,t),\phi) \right] + P V_0, \end{aligned} \tag{A8}$$

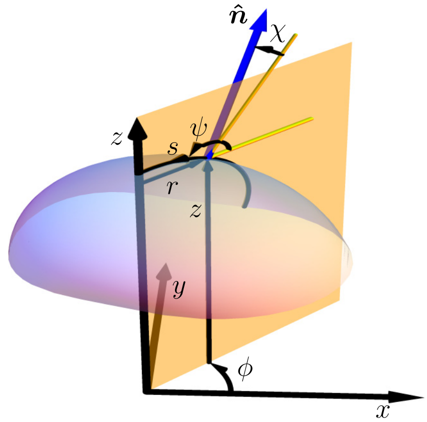

FIG. 8. System of coordinates used for the numerical calculation of the exact shape of the drop.

where we assume that the substrate can be parametrized as $z = g(r, \phi)$. Similarly, the dissipation function (5) can be written as

$$\mathcal{W} = \frac{1}{2}\zeta \int_0^{2\pi} d\phi \, \frac{r\dot{r}^2\left(1 + g_r^2 + \frac{1}{r^2}g_\phi^2\right)}{\sqrt{1 + \frac{1}{r^2}\left[r_\phi^2 + (g_r r_\phi + g_\phi)^2\right]}}. \tag{A9}$$

To take into account the constraints (A4)–(A6), we introduce the Lagrange fields $\mu(u, \phi, t)$, $\nu(u, \phi, t)$, and $\xi(u, \phi, t)$ and we add to the free energy (A8) the Lagrangian

$$\mathcal{F}_L = \int_0^{2\pi} d\phi \int_0^1 du[\mu(r_u - s_0 \cos\psi) + \nu(z_u - s_0 \sin\psi) + \xi(r \tan\chi + \sin\psi r_\phi - \cos\psi z_\phi)]. \tag{A10}$$

As in Sec. VI, the dynamical equations of the droplet are found by setting to zero the variation $\delta(\dot{\mathcal{F}} + \dot{\mathcal{F}}_L + \mathcal{W})$ of the total Rayleighian with respect to the generalized speeds $\dot{r}$, $\dot{z}$, $\dot{s}_0$, $\dot{\psi}$, $\dot{\chi}$, $\dot{P}$, $\dot{\mu}$, $\dot{\nu}$, and $\dot{\xi}$, that we can consider as independent thanks to the Lagrangian (A10). By integrating by parts, we then obtain the bulk equations

$$\mu_u = \frac{\gamma s_0}{\cos\chi} - P r s_0 \sin\psi + \xi \tan\chi - \frac{\partial}{\partial\phi}(\xi \sin\psi), \tag{A11}$$

$$\nu_u = \frac{\partial}{\partial\phi}(\xi \cos\psi), \tag{A12}$$

$$\mu s_0 \sin\psi - \nu s_0 \cos\psi = \frac{1}{2} P r^2 s_0 \cos\psi - \xi(\cos\psi r_\phi + \sin\psi z_\phi), \tag{A13}$$

$$\xi = -\gamma s_0 \sin\chi, \tag{A14}$$

plus the three constraints (A4)–(A6). These bulk equations are accompanied by the boundary conditions

$$\int_0^1 du\left(\frac{\gamma r}{\cos\chi} - \frac{1}{2} P r^2 \sin\psi - \mu\cos\psi - \nu \sin\psi\right) = 0, \tag{A15}$$

$$V_0 = \int_0^{2\pi} d\phi \left\{ \int_0^1 du \frac{1}{2} r^2 s_0 \sin\psi + \int_0^{2\pi} d\phi \int_0^{r(u=0,\phi,t)} dr\, r[z(u=0,\phi,t) - g(r,\phi)] \right\}, \tag{A16}$$

$$\left[\frac{\zeta r\dot{r}\left(1+g_r^2+\frac{1}{r^2}g_\phi^2\right)}{\sqrt{1+\frac{1}{r^2}\left[r_\phi^2+(g_r r_\phi+g_\phi)^2\right]}}-\frac{1}{2}Pr^2 g_r-\mu-\nu g_r-\gamma\cos\Phi_Y r\sqrt{1+g_r^2+\frac{1}{r^2}g_\phi^2}\right]_{u=0}=0, \tag{A17}$$

$$z(u=0,\phi,t)=g(r(u=0,\phi,t),\phi), \tag{A18}$$

$$r(u=1,\phi,t)=0, \tag{A19}$$

$$z(u=1,\phi,t)=z_0(t), \tag{A20}$$

$$\int_0^{2\pi}\nu(u=1,\phi,t)\,d\phi=0, \tag{A21}$$

where Eq. (A18) is the contact condition between the drop and the substrate and we have taken into account that for $u=1$, corresponding to the top of the droplet, $r(u=1,\phi,t)=0$ and $z(u=1,\phi,t)=z_0(t)$, where the unknown height z_0 is independent of ϕ.

1. Elimination of the Lagrange fields

At a given time t, the bulk equations (A4)–(A6) and (A11)–(A14) express the equilibrium conditions for the surface of the droplet. Therefore, they can also be obtained from the Lagrange equations [19]

$$\frac{\partial}{\partial u}\left(\frac{\partial\mathcal{L}}{\partial\boldsymbol{q}_u}\right)+\frac{\partial}{\partial\phi}\left(\frac{\partial\mathcal{L}}{\partial\boldsymbol{q}_\phi}\right)-\frac{\partial\mathcal{L}}{\partial\boldsymbol{q}}=0, \tag{A22}$$

that correspond to the minimization of the free energy

$$\int_0^{2\pi}d\phi\int_0^1 du\,\mathcal{L}(\boldsymbol{q},\boldsymbol{q}_u,\boldsymbol{q}_\phi,\phi) \tag{A23}$$

with respect to the Lagrangian coordinates

$$\boldsymbol{q}=(r,z,\psi,\chi,\mu,\nu,\xi), \tag{A24}$$

where the Lagrangian density

$$\begin{aligned}\mathcal{L}=&\frac{\gamma r s_0}{\cos\chi}-\frac{1}{2}Pr^2 s_0\sin\psi+\mu(r_u-s_0\cos\psi)\\&+\nu(z_u-s_0\sin\psi)+\xi(r\tan\chi+\sin\psi\, r_\phi-\cos\psi\, z_\phi)\end{aligned} \tag{A25}$$

coincides with the integrand of the double integral in ϕ and u in the free energy $\mathcal{F}+\mathcal{F}_L$ [see Eqs. (A8) and (A10)]. Then, since $\mathcal{L}$ does not depend explicitly on u [30], it follows from the equilibrium equations (A22) that the Hamiltonian density

$$\mathcal{H}=\frac{\partial\mathcal{L}}{\partial\boldsymbol{q}_u}\cdot\boldsymbol{q}_u-\mathcal{L} \tag{A26}$$

satisfies the relation [31]

$$\frac{\partial\mathcal{H}}{\partial u}=-\frac{\partial}{\partial\phi}\left(\frac{\partial\mathcal{L}}{\partial\boldsymbol{q}_\phi}\cdot\boldsymbol{q}_u\right). \tag{A27}$$

Now, according to Eq. (A25),

$$\frac{\partial}{\partial \phi}\left(\frac{\partial \mathcal{L}}{\partial \boldsymbol{q}_\phi} \cdot \boldsymbol{q}_u\right) = \xi(\sin\psi\, r_u - \cos\psi\, z_u), \tag{A28}$$

and the right-hand side of this equation is zero for the equilibrium solutions, because of Eqs. (A4) and (A5). Therefore, according to Eq. (A27), the Hamiltonian density does not depend on u: $H = H(\phi, t)$. From the definition (A26), the latter is equal to

$$\mathcal{H}(\phi, t) = -\frac{\gamma r s_0}{\cos\chi} + \frac{1}{2} P r^2 s_0 \sin\psi + \mu s_0 \cos\psi + \nu s_0 \sin\psi + \xi(r\tan\chi + \sin\psi\, r_\phi - \cos\psi\, z_\phi). \tag{A29}$$

From the constraint (A6), the term multiplying ξ in the right-hand side of Eq. (A29) is zero. Moreover, since $s_0 = s_0(\phi, t)$ does not depend on u, from the boundary condition (A15) we obtain the constraint

$$\frac{\gamma r}{\cos\chi} - \frac{1}{2} P r^2 \sin\psi - \mu\cos\psi - \nu\sin\psi = 0, \tag{A30}$$

meaning that the conserved Hamiltonian density is zero. The three algebraic equations (A13), (A14), and (A30) allow us to express the three Lagrange fields μ, ν, and ξ in terms of the other Lagrange coordinates and thus to eliminate them from the equations describing the dynamical evolution of the drop.

2. Evolution equations

By eliminating the Lagrange fields, we obtain the bulk equations [31]

$$r_u = s_0 \cos\psi, \tag{A31}$$

$$z_u = s_0 \sin\psi, \tag{A32}$$

$$\psi_u = s_0 \frac{\frac{\bar{P}}{\cos^3\chi} - \frac{\chi_\phi + \sin\psi}{r\cos^2\chi} + \frac{(\cos\psi\, r_\phi + \sin\psi\, z_\phi)(\psi_\phi - \cos\psi\tan\chi)}{r^2}}{1 + \frac{1}{r^2}\left(r_\phi^2 + z_\phi^2\right)}, \tag{A33}$$

where $\bar{P} = P/\gamma$ is the reduced pressure difference and the angle χ is given by Eq. (A6) [32]. The boundary conditions at $u = 0$ (corresponding to the contact line) are

$$z(u = 0, \phi, t) = g(r(u = 0, \phi, t), \phi), \tag{A34}$$

$$\dot{r}|_{u=0} = \frac{\gamma}{\zeta}\sqrt{1 + \frac{1}{r^2}\left(r_\phi^2 + z_\phi^2\right)}\Bigg|_{u=0} \left\{ \frac{\cos\Phi_Y}{\sqrt{1 + g_r^2 + \frac{1}{r^2} g_\phi^2}} + \left[\frac{1}{\cos\chi}(\cos\psi + \sin\psi\, g_r) + \frac{\sin\chi}{r}(\sin\psi\, z_\phi + \cos\psi\, r_\phi)(\sin\psi - \cos\psi\, g_r)\right]\left(1 + g_r^2 + \frac{1}{r^2} g_\phi^2\right)^{-1} \right\}_{u=0}, \tag{A35}$$

while the boundary conditions at $u = 1$ (intersection of the drop with the z axis) are

$$r(u = 1, \phi, t) = 0, \tag{A36}$$

$$z(u = 1, \phi, t) = z_0(t), \tag{A37}$$

$$\int_0^{2\pi} d\phi \left[\frac{r \sin\psi}{\cos\chi} - \frac{1}{2}\bar{P} r^2 - \sin\chi \cos\psi (\cos\psi\, r_\phi + \sin\psi\, z_\phi) \right]_{u=1} = 0, \tag{A38}$$

where $z_0(t)$ is an unknown height independent of ϕ. One final boundary condition is provided by the volume constraint (A16).

3. Numerical scheme

To cope with the unknown length $s_0(\phi, t)$ of the curve intersection between the surface of the drop and the half-plane $\phi =$ const, we treat s_0 as an extra integration field $s_0(u, \phi, t)$ that obeys the differential equation

$$\frac{\partial s_0}{\partial u} = 0 \tag{A39}$$

that states that s_0 does not depend on u. Similarly, to impose the constant volume constraint (A16), we treat the volume V as a function of u and t, $V = V(u, t)$, satisfying the differential equation

$$\frac{\partial V}{\partial u} = \int_0^{2\pi} d\phi \left(\frac{1}{2} s_0 r^2 \sin\psi \right), \tag{A40}$$

with the boundary conditions

$$V(u = 0, t) = \int_0^{2\pi} d\phi \int_0^{r(u=0,\phi,t)} dr\, r[z(u = 0, \phi, t) - g(r, \phi)], \tag{A41}$$

$$V(u = 1, t) = V_0. \tag{A42}$$

Finally, the unknown reduced pressure $\bar{P}(t)$ is determined by treating it as an additional integration variable satisfying the differential equation

$$\frac{\partial \bar{P}}{\partial u} = 0. \tag{A43}$$

We now express the fields $r(u, \phi, t)$, $z(u, \phi, t)$, $\psi(u, \phi, t)$, and $s_0(u, \phi, t)$ in terms of their Fourier coefficients $\hat{r}_n$, $\hat{z}_n$, $\hat{\psi}_n$, and $\hat{s}_{0n}$ with respect to the cyclic variable ϕ. Explicitly, for a given real periodic function $f(\phi)$, we set [33]

$$f(\phi) = \frac{1}{\sqrt{N}} \left\{ \hat{f}_0 + \sum_{n=1}^{\lceil \frac{N}{2} - 1 \rceil} [\hat{f}_n \exp(in\phi) + \text{c.c.}] + \hat{f}_{N/2} \cos\left(\frac{N}{2}\phi \right) \right\}, \tag{A44}$$

where $\lceil x \rceil$ is the smallest integer $\geqslant x$, $\hat{f}_{N/2}$ exists only if N is even, and c.c. indicates complex conjugate. The number N is the total number of real components of the Fourier harmonics. This truncated Fourier series can be inverted to obtain the Fourier amplitudes $\hat{f}_m$, for $m = 0, 1, \ldots, \lfloor \frac{N}{2} \rfloor$, where $\lfloor x \rfloor$ is the largest integer $\leqslant x$. To this aim, we introduce the values $f_n = f(\phi_n)$ of the function $f(\phi)$ at the discrete angles

$$\phi_n = n\frac{2\pi}{N} \quad \text{for } n = 0, 1, \ldots, N - 1. \tag{A45}$$

Then,

$$\hat{f}_m = \frac{1}{\sqrt{N}} \sum_{n=0}^{N-1} f_n \exp(-in\phi_m). \tag{A46}$$

Note that $\hat{f}_0$, and $\hat{f}_{N/2}$ if N is even, are real, while all the other harmonics are complex. In total, we thus have as many real coefficients in the Fourier space (N) as discrete values f_n in the real space.

We apply this discrete Fourier transform to the bulk equations (A31)–(A33) and (A39), thus obtaining a set of $4N$ coupled ordinary differential equations in the independent variable u for the real and imaginary parts of the Fourier harmonics of the profile

$$\frac{d\hat{r}_n}{du} = \hat{f}_{rn}, \tag{A47}$$

$$\frac{d\hat{z}_n}{du} = \hat{f}_{zn}, \tag{A48}$$

$$\frac{d\hat{\psi}_n}{du} = \hat{f}_{\psi n}, \tag{A49}$$

$$\frac{d\hat{s}_{0n}}{du} = 0, \tag{A50}$$

where $\hat{f}_{rn}$, $\hat{f}_{zn}$, and $\hat{f}_{\psi n}$, for $n = 0, 1, \ldots, \lfloor \frac{N}{2} \rfloor$, are the nth harmonics of the discrete transform (A46) of the right-hand-sides of Eqs. (A31)–(A33), respectively. They are obtained numerically by performing all nonlinear operations in the direct space in correspondence to the discrete angles ϕ_n, and all the derivatives with respect to ϕ in the Fourier space.

The dynamics of the contact line is contained in Eq. (A35). To ensure that the droplet remains centered with respect to our cylindrical coordinate system, we rewrite this dynamical equation in a frame moving with an instantaneous speed v_x (respectively, v_y) in the x (respectively, y) direction. In such a frame, the radial speed of the contact line becomes

$$\dot{r}|_{u=0} = v_r - v_x \cos\phi - v_y \sin\phi + \left.\frac{r_\phi}{r}\right|_{u=0} (v_y \cos\phi - v_x \sin\phi), \tag{A51}$$

where the radial speed v_r is given by the right hand-side of Eq. (A35). At any given time t, we determine the speeds $v_x(t)$ and $v_y(t)$ by imposing that the $n = 1$ Fourier harmonics of the right-hand side of Eq. (A51) are zero. Indeed, when the $n > 0$ Fourier harmonics of the contact line are small, the $n = 1$ harmonics represent a rigid translation. We take the values of $v_x(t)$ and $v_y(t)$ determined in this way as the speed of the contact line.

The numerical solution of the dynamics of the drop now proceeds as follows. We start at $t = t_0$ from an initial shape of the contact line, i.e., a given set of harmonics $\hat{r}_n(u = 0, t = t_0)$, and we integrate numerically the $N - 2$ differential equations with given initial conditions for $\dot{\hat{r}}_n$ obtained by computing the discrete Fourier transform of Eq. (A51) (the two equations for the two real components of the first harmonic can be omitted as these components remain constant). To this aim, for each given set of harmonics $\hat{r}_n(u = 0, t)$, we must compute the corresponding right-hand side of Eq. (A35), i.e., the values of $z(u = 0, \phi, t)$ and $\psi(u = 0, \phi, t)$. These values are obtained by computing the full shape of the drop for the given contact line, which amounts to solving the $4N + 2$ equations (A47)–(A50), (A40), and (A43) with $2N + 1$ boundary conditions at $u = 0$ [the N conditions (A34), the scalar constraint (A41), and the N given real components of the harmonics $\hat{r}_n(u = 0, t = t_0)$], and the $2N + 1$ boundary conditions at $u = 1$ (A36)–(A38) and (A42). Note that since $z_0(t)$ is unknown, Eq. (A37) gives only $N - 1$ boundary conditions, namely the cancellation of the nonzero harmonics of $z(u = 1, \phi, t)$: $\hat{z}_n(u = 1, t) = 0$ for $n \neq 0$. Note also that our boundary problem has an apparent singularity at $u = 1$ coming from the singularity of the cylindrical coordinates [see Eqs. (A33) and (A6)], since $r(u = 1, \phi, t) = 0$. To avoid this singularity, we impose the boundary conditions not at $u = 1$ but at $u = 1 - \epsilon$, with $0 < \epsilon \ll 1$, by developing to first order in ϵ r, z, ψ, and V with the help of Eqs. (A31)–(A33), (A39), and (A40). Equations (A36), (A37), and (A42) are then replaced, respectively, by the conditions

$$r(u = 1 - \epsilon, \phi, t) = -\epsilon s_0 \cos\psi|_{u=1-\epsilon}, \tag{A52}$$

$$z(u = 1 - \epsilon, \phi, t) = z_0(t) - \epsilon s_0 \sin\psi|_{u=1-\epsilon}, \tag{A53}$$

$$V(u = 1 - \epsilon, t) = V_0 - \epsilon \int_0^{2\pi} d\phi \left(\frac{1}{2} s_0 r^2 \sin\psi \right)_{u=1-\epsilon}, \tag{A54}$$

while Eq. (A38), to first order, continues to be satisfied at $u = 1 - \epsilon$.

The dynamical equations are integrated by means of variable step variable order backward differentiation formulae [34] to take into account of the stiff nature of the problem (the higher the harmonic, the smaller the relaxation time). The boundary value problem is integrated by means of a finite difference scheme with deferred correction and Newton iteration on an adaptive mesh [35]. The discrete Fourier transforms are computed with a fast Fourier algorithm [36]. We increase the value N of the total number of real components of the Fourier harmonics until the solution converges to the desired precision. For the presented results, N varies between 32 and 64. Also, note that all the nonlinear calculations in real space are usually performed with a number of Fourier components greater than the number of components that are retained for the integration of the equations, to avoid aliasing effects [36].

4. Horizontal force on the drop

We compute the total horizontal force acting on the drop according to Eq. (62), with the stress tensor (60). With our parametrization of the surface of the drop, it can be easily shown that

$$\begin{aligned} F_x = \gamma \int_0^{2\pi} d\phi \Bigg\{ & \frac{\cos\chi}{\cos\psi} \left(\frac{\tan\chi}{r} r_\phi - \sin\psi \right) [r \cos\phi (\sin\psi - \cos\psi\, g_r) + \sin\phi (\cos\psi\, g_\phi - r \tan\chi)] \\ & + (r\cos\phi + r_\phi \sin\phi) \left[\cos\Phi_Y \sqrt{1 + g_r^2 + \frac{1}{r^2} g_\phi^2} + \frac{1}{\cos\chi \cos\psi} \right] \Bigg\}_{u=0}, \end{aligned} \tag{A55}$$

$$\begin{aligned} F_y = \gamma \int_0^{2\pi} d\phi \Bigg\{ & \frac{\cos\chi}{\cos\psi} \left(\frac{\tan\chi}{r} r_\phi - \sin\psi \right) [r \sin\phi (\sin\psi - \cos\psi\, g_r) - \cos\phi (\cos\psi\, g_\phi - r \tan\chi)] \\ & + (r\sin\phi - r_\phi \cos\phi) \left[\cos\Phi_Y \sqrt{1 + g_r^2 + \frac{1}{r^2} g_\phi^2} + \frac{1}{\cos\chi \cos\psi} \right] \Bigg\}_{u=0}. \end{aligned} \tag{A56}$$

[1] L. D. Landau, *Fluid Mechanics* (Pergamon, London, 1959).

[2] J. Thomson, XLII. On certain curious motions observable at the surfaces of wine and other alcoholic liquors, The London, Edinburgh, and Dublin Philosophical Magazine and Journal of Science **10**, 330 (1855).

[3] C. Marangoni, Ueber die Ausbreitung der Tropfen einer Flüssigkeit auf der Oberfläche einer anderen, Ann. Phys. **219**, 337 (1871).

[4] T. Ondarçuhu and M. Veyssié, Dynamics of spreading of a liquid drop across a surface chemical discontinuity, J. Phys. II France **1**, 75 (1991).

[5] M. M. Weislogel, Steady spontaneous capillary flow in partially coated tubes, AIChE J. **43**, 645 (1997).

[6] C. D. Bain, G. D. Burnett-Hall, and R. R. Montgomerie, Rapid motion of liquid drops, Nature (London) **372**, 414 (1994).
[7] F. D. Dos Santos and T. Ondarçuhu, Free-Running Droplets, Phys. Rev. Lett. **75**, 2972 (1995).
[8] M. K. Smith, Thermocapillary migration of a two-dimensional liquid droplet on a solid surface, J. Fluid Mech. **294**, 209 (1995).
[9] E. Lorenceau and D. Quéré, Drops on a conical wire, J. Fluid Mech. **510**, 29 (2004).
[10] C. Lv, C. Chen, Y.-C. Chuang, F.-G. Tseng, Y. Yin, F. Grey, and Q. Zheng, Substrate Curvature Gradient Drives Rapid Droplet Motion, Phys. Rev. Lett. **113**, 026101 (2014).
[11] H. Bouasse, *Capillarité, phénomènes superficiels* (Delagrave, Paris, 1924).
[12] P. G. de Gennes, Wetting: Statics and dynamics, Rev. Mod. Phys **57**, 827 (1985).
[13] B. W. Cherry and C. M. Holmes, Kinetics of wetting of surfaces by polymers, J. Colloid Interface Sci. **29**, 174 (1969).
[14] T. D. Blake and J. M. Haynes, Kinetics of liquid/liquid displacement, J. Colloid Interface Sci. **30**, 421 (1969).
[15] M. J. de Ruijter, J. D. Coninck, and G. Oshanin, Droplet spreading: Partial wetting regime revisited, Langmuir **15**, 2209 (1999).
[16] T. D. Blake, The physics of moving wetting lines, J. Colloid Interface Sci. **299**, 1 (2006).
[17] C. W. Extrand and Y. Kumagai, Liquid drops on an inclined plane: The relation between contact angles, drop shape, and retentive force, J. Colloid Interface Sci. **170**, 515 (1995).
[18] Nan Gao, F. Geyer, D. W. Pilat, S. Wooh, D. Vollmer, H.-J. Butt, and R. Berger, How drops start sliding over solid surfaces, Nat. Phys. **14**, 191 (2018).
[19] H. Goldstein, C. Poole, and J. Safko, *Classical Mechanics*, 3rd ed. (Addison-Wesley, San Francisco, 2001).
[20] M. Doi, Onsager's variational principle in soft matter, J. Phys.: Condens. Matter **23**, 284118 (2011).
[21] S. Singer and S. Singer, Efficient implementation of the Nelder-Mead search algorithm, Appl. Num. Anal. Comp. Math. **1**, 524 (2004).
[22] T. D. Blake, in *Wettability*, edited by J. C. Berg (Dekker, New York, 1993), p. 251.
[23] M. J. de Ruijter, J. De Coninck, T. D. Blake, A. Clarke, and A. Rankin, Contact angle relaxation during the spreading of partially wetting drops, Langmuir **13**, 7293 (1997).
[24] See Supplemental Material at http://link.aps.org/supplemental/10.1103/PhysRevFluids.3.103601 for movies of the dynamical evolution of the droplet according to our numerical solution.
[25] The results, expressed by Eqs. (38)–(40), are valid whatever the value of $\theta(\phi, t)$.
[26] M. Abramowitz and I. A. Stegun, *Handbook of Mathematical Functions with Formulas, Graphs, and Mathematical Tables* (Dover, New York, 1970).
[27] E. Kreyszig, *Differential Geometry* (Dover, New York, 1991).
[28] Note that in this section the parameter r denotes the distance to the z axis and not, as in Sec. VI, the distance to the origin.
[29] P. Galatola and J.-B. Fournier, Capillary force acting on a colloidal particle floating on a deformed interface, Soft Matter **10**, 2197 (2014).
[30] Note that, on the other hand, the Lagrangian density explicitly depends on ϕ through the function $s_0(\phi, t)$.
[31] P. Galatola, Capillary force and torque on spheroidal particles floating at a fluid interface beyond the superposition approximation, Phys. Rev. E **93**, 022604 (2016).
[32] Note that, with respect to Ref. [31], here the angle χ has opposite sign, because of the different orientation of the normal to the liquid surface.
[33] R. W. Hamming, *Numerical Methods for Scientists and Engineers* (Dover, New York, 1987).
[34] U. M. Ascher and L. R. Petzold, *Computer Methods for Ordinary Differential Equations and Differential-Algebraic Equations* (Siam, Philadelphia, 1998).
[35] U. M. Ascher, R. M. M. Mattheij, and R. D. Russell, *Numerical Solution of Boundary Value Problems for Ordinary Differential Equations* (Prentice-Hall, Englewood Cliffs, NJ, 1988).
[36] E. O. Brigham, *The Fast Fourier Transform and Its Applications* (Prentice Hall, Upper Saddle River, NJ, 1988).